ANALYSIS OF HYDRODYNAMIC LIFT FOR
GAS TURBINE OIL BRUSH SEALS

By
ERTUĞRUL ÇETİNSOY

Submitted to the Graduate School of Engineering and Natural Sciences
in partial fulfillment of
the requirements for the degree of
Master of Science

SABANCI UNIVERSITY
Spring 2006

ANALYSIS OF HYDRODYNAMIC LIFT FOR

GAS TURBINE OIL BRUSH SEALS

APPROVED BY:

Associate Prof. Dr. MAHMUT F. AKŞİT   ....
   (Dissertation Advisor)

Prof. Dr. ASIF ŞABANOVİÇ   ....

Assistant Prof. Dr. SERHAT YEŞİLYURT   ....

Assistant Prof. Dr. GÜLLÜ KIZILTAŞ ŞENDUR   ....

Assistant Prof. Dr. İLYAS KANDEMİR   ....

DATE OF APPROVAL: ....

ANALYSIS OF HYDRODYNAMIC LIFT FOR GAS TURBINE OIL BRUSH SEALS

Ertuğrul ÇETİNSOY

EECS, M.Sc. Thesis, 2006

Thesis Supervisor: Associate Prof. Dr. Mahmut F. AKŞİT

ABSTRACT

Brush seals are used in gas turbine engine applications for their effectiveness in controlling leakage flows between stationary parts and rotating shaft. With their superior leakage performance, they are becoming the successor to the labyrinth seals, which have always been widely used since the first gas turbine engines. After gaining popularity in secondary flow air sealing, applications extended to more challenging oil and oil mist sealing locations.

Due to high rotor surface speed oil temperature rise and coking become main issues in addition to leakage performance. While each bristle forms very small bearing surface, high rotor surface speed and viscous sealing medium provide sufficient hydrodynamic lift force to overcome bristle reaction forces. The gap generated between the bristle tips and the rotor surface determines the oil temperature rise and leakage rate. Due to shear thinning in oil sealing applications lift force is inversely correlated to oil temperature rise leading to a self-balancing effect with surface speed. The aim of a proper design for oil brush seals would be to keep the leakage at the minimum rate while avoiding excess oil temperature rise.

Inherent complexity of bristles make calculation of hydrodynamic lift forces under a brush seal rather complicated. To avoid costly experimental investigations, a closed form analytical solution would prove very useful to compare candidate designs

and to study what-if scenarios. This work investigates analytical solutions to hydrodynamic lift clearance and bristle lift forces based on bearing theory. After a detailed discussion on short bearing approach, possible closed form solutions based on long bearing approach have been explored. A more comprehensive yet numerical solution based on finite bearing approach has also been provided to compare and understand pressure and lifting force results. Analyses have been performed for effective constant oil viscosity. Shear thinning effect has been later introduced through use of published oil temperature data for various rotor surface speeds. As bristle tip clearance data are not available, validity of analytical the results have been evaluated using beam bending forces and experimental leakage flow data for various surface speeds. The results indicate that long bearing solution underestimates the oil lift force. Although more comprehensive, finite bearing solution requires the knowledge of axial deflection/bloom of the bristle pack. Simple yet functional, short bearing solution appears as a viable tool for seal designers to compare various seal designs before doing detail experimental evaluation on a plausible candidate. Finally, possible further work areas have been discussed.

GAZ TÜRBİNİ FIRÇA YAĞ KEÇELERİNİN HİDRODİNAMİK KALDIRMA KUVVETİ ANALİZİ

Ertuğrul ÇETİNSOY

EECS, Yüksek Lisans Tezi, 2006

Tez Danışmanı: Doç. Dr. Mahmut F. AKŞİT

Anahtar Kelimeler: Fırça keçe, hidrodinamik yağ kaldırması, yağ yalıtımı, uzun yatak, kısa yatak, sonlu yatak, aşağı üfleme, fırça tel ucu yüksekliği, yağ kaçağı

ÖZET

Fırça keçeler sabit ve dönen parçalar arasındaki kaçak akışları denetlemekteki etkinlikleri nedeniyle gaz turbini sızdırmazlık uygulamalarında kullanılmaktadır. Üstün sızdırmazlık yetenekleri nedeniyle, ilk gaz türbinlerinden beri bu iş için yaygın olarak kullanılmış olan labirent keçelerin yerini almaktadır. İkincil hava akış sızdırmazlığı görevinde bir çok başarılı uygulamadan sonra, fırça keçeler daha sorunlu olan yağ ve yağ buharı kaçaklarının önlenmesi amacıyla da kullanılmaya başlanmıştır.

Yüksek yüzey hızı nedeniyle bu uygulamalarda yağ sıcaklığının artması ve yağ yanması sızdırmazlık performansına eklenen ana problemlerdir. Küçük fırça telleri hidrodinamik yağ kaldırması için çok küçük bir kaldırma yüzeyi sunsa da, yüksek yüzey hızı ve yağın yüksek viskozitesi fırçada var olan reaksiyon kuvvetlerini yetebilecek seviyede hidrodinamik kaldırma kuvveti oluşmasına neden olmaktadır. Fırça tellerinin uçları ve mil yüzeyi arasında oluşan boşluğun yüksekliği yağ sıcaklığı artışını ve kaçak akış miktarını belirlemektedir. Yağ yalıtımı uygulamalarında yağın vizkozitesinden dolayı ısınmasınarak incelmesi nedeniyle kaldırma kuvveti yağ sıcaklığı artışıyla ters bir bağıntıya sahiptir. Bu yüzden de hız arttıkça artan kaldırma kuvveti, ısınarak incelen yağın düşen viskositesi ile dengelenmektedir. Fırça yağ keçelerinde doğru tasarımın amacı aşırı yağ sıcaklığı artışına meydan vermeden kaçak akış miktarını en düşük seviyede tutmaktır.

Tellerinin doğasında bulunan karmaşık yapı fırça keçelerin altında oluşan hidrodinamik kaldırma kuvvetlerinin hesaplanmasını oldukça zor kılmaktadır. Pahalı deneysel araştırmalardan kaçınmak için kapalı formda bir analitik çözümün bulunması aday tasarımları karşılaştırma ve olası bütün çözümleri incelemede kullanışlı olacaktır. Bu çalışma yağlama teorisine dayalı olarak hidrodinamik kaldırma mesafesi ve fırça teli kaldırma kuvvetlerini incelemektedir. Kısa yatak kabulü üstüne detaylı bir anlatımdan sonra, uzun yatak kabulüne dayalı olası bir kapalı form çözüm araştırılmıştır. Basınç ve kaldırma kuvveti sonuçlarını anlamak için sonlu yatak kabulüne dayalı daha geniş fakat numerik bir çözüm de sağlanmıştır. Analizler sabit etkin yağ viskozitesi kabulüne dayalı olarak yapılmıştır. Yağın viskozitesinden dolayı ısınmasıyla incelmesinin etkisi, çeşitli yüzey hızları için yayınlanmış olan yağ sıcaklığı verileri kullanılarak ayrıca eklenmiştir. Hidrodinamik kaldırma dolayısıyla oluşan fırça teli ucunun mil yüzeyinden uzaklığı ölçülemediği için, analitik sonuçların geçerliliği tel eğilme kuvvetleri ve çeşitli mil hızlarında denenmiş kaçak akış verilerine göre değerlendirilmiştir. Sonuçlar uzun yatak yaklaşımına dayanan çözümün yağın kaldırma kuvvetini çok düşük hesapladığını göstermektedir. Daha ayrıntılı olmasına rağmen sonlu yatak yaklaşımına dayanan çözüm, fırça grubundaki eksenel açılmanın seviyesinin bilinmesini gerektirmektedir. Basit ama fonksiyonel olan kısa yatak yaklaşımına dayanan çözüm, tasarımcılarının çeşitli keçe tasarımları arasında karşılaştırma yaparak deney yapmadan en iyi adayı bulmalarına yardımcı olabilecek uygun bir yöntem olarak görünmektedir. Son olarak, ilerisi için çalışma alanları da tartışılarak sunulmuştur.

To my country, Türkiye…

ACKNOWLEDGEMENTS

TABLE OF CONTENTS

LIST OF FIGURES

LIST OF TABLES

TABLE OF SYMBOLS

x,y,z	World coordinates
μ	Viscosity (Pa-s)
T	Temperature (C)
U	Rotor surface speed (m/s)
h	Clearance between bristle and rotor surfaces
H	Minimum clearance between bristle and rotor surface
X_{bloom}	Blooming distance between the bristles in rotation direction
Y_{bloom}	Axial blooming distance between the bristles
LimitLow	Function of X coordinate of the previous bristle's surface for a Y value
LimitHigh	Function of X coordinate of the lifted bristle's surface for a Y value
hhigh	Height of the upper surface of the bristle
hlow	Height of the lower surface of the bristle
d	Bristle diameter
R_b	Bristle radius
R_a	Rotor radius
R_A	Radius for bristle curvature
θ	Cant (bristle lay) angle
W	Hydrodynamic lift force
P	Pressure
P_a	Ambient pressure
ρ	Oil density
V_x, V_y, V_z	Speed of the oil particle in coordinate axis directions
t	Time
g_x, g_y, g_z	Acceleration in coordinate axis directions
B, L	Width and length of the bearing
Re	Reynolds number
x^*, z^*	Normalized coordinates
V_x^*, V_z^*	Normalized speeds in coordinate axis directions
t^*	Normalized time
P^*	Normalized pressure
Re^*	Normalized Reynolds number

TABLE OF ABBREVIATIONS

CFD	Computational Fluid Dynamics
EDM	Electro Discharge Machining
BH	Bristle height
FH	Fence height

1   INTRODUCTION AND PROBLEM STATEMENT

1.1   Introduction

A gas turbine is a combustion engine that mainly consists of compressor and turbine stages which are coupled by a shaft with a fuel combustor in-between. When shaft rotates, the axial compressor provides continuous air flow into the combustor. Fuel is injected into the hot, compressed air in the combustor where combustion takes place. Expanding combustion gas delivers energy to the rotating turbine while flowing towards aft to the exhaust. After it is run once, gas turbine keeps rotating as long as air and fuel are supplied.

Gas turbines are used mainly in propulsion for air, space and some sea crafts and electrical power generation on the land. They are highly efficient machines (currently up to 60% combined cycle efficiency) with high power-to-weight and power-to-size ratio, which makes them appealing. However, their high manufacturing and maintenance costs render them economical to operate only above certain power levels (around 2MW). Still, gas turbines constitute an economical way to generate large amount of energy and their persistently increasing efficiency seem to be appreciated more in the future, when oil and natural gas prices will increase due to shortage.

To increase the efficiency of gas turbines, an effective and economic approach is to prevent parasitic leakages [1]. These are mainly the primary leakage flows between blade tips and the stator, and the secondary flow leakages of oil, oil mist and air in the inner section of the gas turbines [2]. The secondary flows in the gas turbines are not the main combustion hot gas flow; instead they are comprised of cooling air flows, purge flows, and oil/oil mist flows at bearings.

Oil sealing is mostly needed around the bearings at oil sumps to prevent oil consumption or contamination of the downstream parts [3]. The results of such a flow varies from the reduction of efficiency and life-time deteriorating change in the airfoil

of the compressor blades to potential fires in the engine [4]. The solutions adopted for secondary flow oil sealing until now have been buffer systems that consume high pressure inlet air for the operation; carbon seals that are expensive and problematic to produce in large dimensions; labyrinth seals that are the most common system, but have large leakage rates and oil rings which require continuous oil flow. Brush seals emerged as a possible alternative since they permit very low leakage and are compliant to the excitations of the rotor [5].
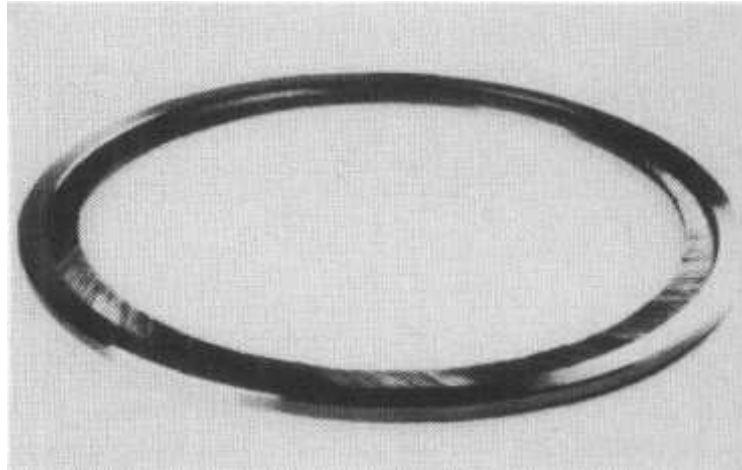
Figure 1: Circular brush seal for an aerospace engine.

A brush seal is a bunch of metallic or nonmetallic bristles that are stowed into a nearly J-sectioned ring. Bristles have a lay angle of around 45º to the normal of the shaft surface [1, 2, 6]. In general, the bristle diameter ranges from 0.05mm to 0.15mm and the bristle density is around 2000 per one inch (25.4mm) seal circumferential length [7]. As illustrated in Figure 2, the long arm of the J is called as "backing plate" forming a support for the bristles against axial bristle deflection the downstream side. The short arm of the J is called as "retaining plate". In most cases, outer ends of the bristles are welded to the ring at the root. Retaining plate clamps the bristles at the root and protects them during assembly and handling. The fence height is determined according to the maximum expected rotor excursions calculated for landing and maneuver deflections in airplanes, and for vibrations and thermal dimensional changes during the startup and cooling of the components of all kinds of turbine engines [2]. Generally there are 8-15 rows of bristles depending on the pressure drop and the fence height. The cant/lay angle between the bristles and the rotor helps for reduction of the friction force between the bristles and the rotor surface [8] and prevents buckling of the bristles during rotor transients.
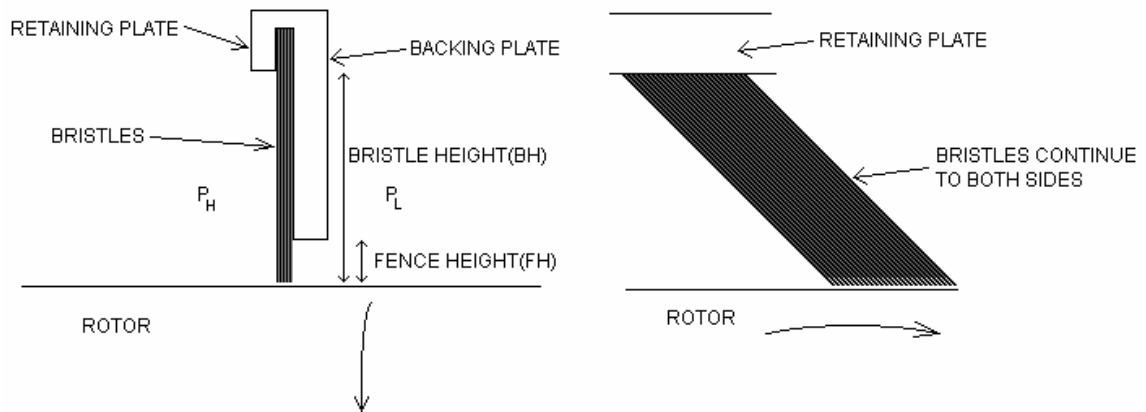
Figure 2: Brush seal structure.

There are mainly three types of leakage flows in a brush seal as shown in Figure 3. One of them is the flow through the bristles and along the backing plate that comes from above the fence height. Another one is the flow through the bristles below the fence height. In this section, the bristles are not supported by the backing plate anymore, so the bristles are not squeezed like above the fence height and a larger flow occurs. The most severe flow occurs between the bristle tips and the rotor surface. In that region, there is no obstacle to penetrate, so any increase in the pressure difference and the clearance between the bristle tips and the rotor surface rapidly increases the rate of leakage flow.
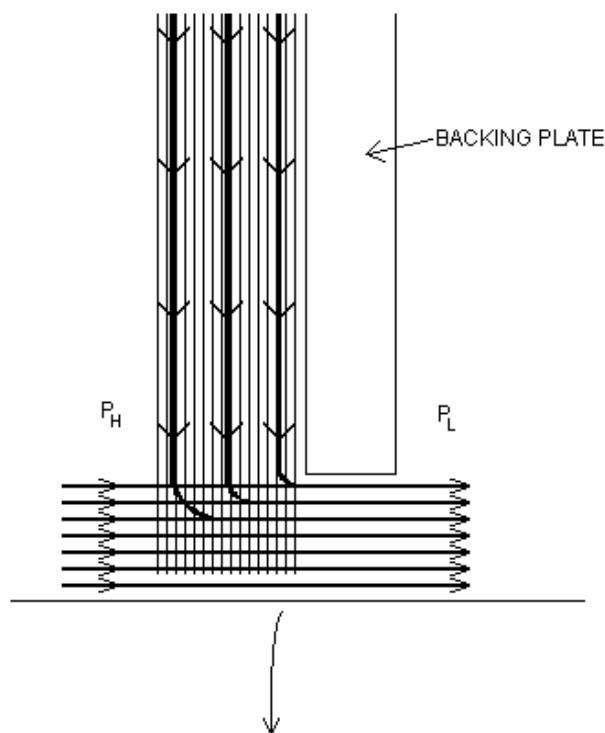
Figure 3: Flows in the brush seal.

During operation, pressure at the high pressure side pushes the bristles to the backing plate. Due to the inter-bristle and bristle to backing plate friction, the pressure load causes the bristles to pack, and to behave like a deformable solid instead of a bunch of free bristles. As a result, the brush seal becomes much stiffer under pressure load and does not comply with the rotor excitations as they would without any pressure load. This can cause severe rubbing between the bristles and rotor surface leading to wear of bristles during a radial excitation of the rotor in to the brush seal. Pressure stiffening effect also lowers sealing performance due to brush hysteresis to follow the rotor that returns to the normal position after an excitation.

A second effect of pressure load on the brush seal is the bristle's being pushed to the rotor surface. This effect is called as "pressure closure" or "blow-down" in the literature. It is anticipated that the existing inward radial flow pushes the bristles to the rotor surface. In the brush pack, the bristles in the high pressure side are less constrained than the bristles in the low pressure side. Due to the pressure pushing the bristles to the downstream side, the low pressure side bristles are confined between the backing plate and the previous bristles in the high pressure side. As a result, the high pressure side bristles are relatively freer in terms of being pushed to the rotor surface with same amount of radial flow. However, the radial flow is driven by the pressure difference between the upper and the lower levels of the bristles and this pressure difference is larger at the low pressure side of the brush seal. This means that although the constraints on the bristles against the radial closure to the rotor are less in the high pressure side, the blow-down force on the bristles are stronger in the low pressure side of the brush seal. For that reason, the effects of blow-down are somehow balanced in the brush seal [7].

1.2   Problem Statement

Although brush seal is a preferable solution for its sealing effectiveness, it does have significant challenges in oil sealing applications. Majority of the previous studies on brush seals aim for air sealing applications with the assumptions of compressible, low viscosity gas flows. However, brush seal oil sealing applications deal with incompressible, lubricating and high viscosity fluid flows. Since nonlinearities coming from compressibility get out of the formulas, incompressible flow simplifies the

calculations in brush seal analyses to some level. The fact that oil is lubricious may also simplify the problem to some extend since it may reduce the hysteresis. Chen et al. [9], Crudgington et al. [10] and Aksit et al. [7] have studied hysteresis phenomena. However, further discussion on hysteresis is out of the scope of this work. Furthermore, the fact that oil is very high viscosity material compared to air simplifies leakage flow analysis for the brush seals eliminating any possibility of turbulence. Duran et al. [11] reported that for a typical oil seal leakage case, normalized Reynolds number is around $1.86*10^{-3}$ which is even much smaller required for any turbulent flow.

However, high viscosity of oil introduces two very significant problems for the brush seals. The first one is controlling the oil temperature and preventing any possible coking. The second one is controlling the hydrodynamic lift and leakage to keep the performance at an acceptable level.

Due to the high viscosity of oil compared to air, shear heating in oil sealing applications becomes a significant problem due to the risk of oil coking on the bristles [4]. Since brush seal permits only a small amount of oil to leak through a very narrow gap, the oil generates a significant level of heat at rotor interface with high shear rate. If not properly designed, this heating may result in some oil to burn resulting in coked particles to stick and coat on the bristle tips. Carbon deposits from coked oil can be very hard. As a result, during the rotor radial excursions bristles can cause severe wear on the rotor surface. Aksit et al. [4], Duran et al. [11], Owen et al. [12], Chew et al. [13] and Dogu et al. [14] studied brush seal temperature profiles. Thermal modeling and calculation of thermal effects are also out of scope of this work. For the viscosity needed in the hydrodynamic lift calculations, the measured temperature test results supplied by Aksit et al. [4] will be used.

As the rotor surface velocity increases, with bristle tips acting as small bearing surfaces oil pressure lifts the bristles of the shaft surface leading to more oil leakage. However, oil viscosity decreases with the shear heat generation due to speed. As a result, as Aksit et al. [4] reported bristle lift and oil leakage stabilizes after certain speed.

The best performance from oil brush seals would be gained in the case when bristle tips are kept at the minimum height from the surface of the rotating shaft without rubbing the surface. To satisfy this aim, the forces on the bristles such as the lift force caused by the rotor-induced oil flow, blow-down force, bristle bending force and other frictional forces, should be known. This work is intended to estimate the hydrodynamic

oil lift force caused by the so-called "circumferential fluid flow" [15]. As reported by Chen et al. [9] it is impossible to get exact values for brush seals. Bristle force balance is a complex total of mainly four effects; lifting force, blow-down force, pressure force and frictional forces.
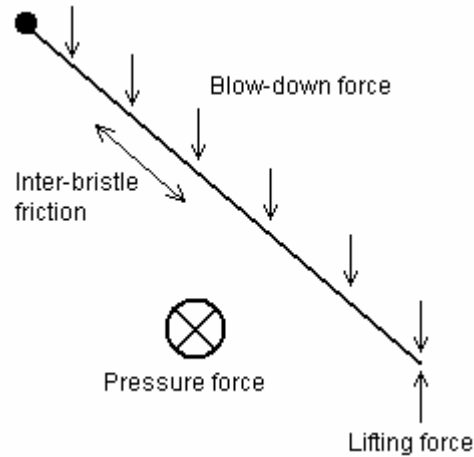
Figure 4: Forces on a brush seal bristle.

These forces include effects from different fields of study: "Fluid flow, solid-fluid interaction, contact mechanics and tribology" [15]. Combining the results taken from these four force estimates is still a problem, because they are also coupled making the problem even more challenging. Dogu et al. [16] made an effort to get a flow solution using bulk porous medium approach. Inherent complexity of brush seals make calculation of hydrodynamic lift forces under a bristles rather complicated. To avoid costly experimental investigations, a simple closed form analytical solution is needed in order to compare candidate designs and to study what-if scenarios. This work investigates possible analytical solutions to hydrodynamic lift clearance and bristle lift forces based on bearing theory. The approach will be to simplify comprehensive Reynolds Equations through application of widely used "Short" and "Long Bearing" assumptions in an attempt to reach for a simple closed form solution for bristle lift. Applicability of simplified solutions will be verified using experimental leakage data through comparison of force results with known bristle beam forces.

2   LITERATURE SURVEY

2.1   General Literature on Turbo Machinery Oil Seals

Secondary flow sealing has been a challenging task ever since the invention of gas turbines. High surface speeds combined with large shaft excursions make sealing of large pressure differentials a difficult engineering problem. Labyrinth seals have been a common solution for a long time. Their most important feature is that their manufacturing is not too complicated and they have low manufacturing costs. They work on the principle of producing leakage flow induced turbulence between the teeth to generate resistance against the flow. The leakage flow rate depends basically on the number of the teeth and the gap between the teeth and the shaft surface [8]. As long as the gap between the teeth and the shaft is reduced, the flow is reduced.
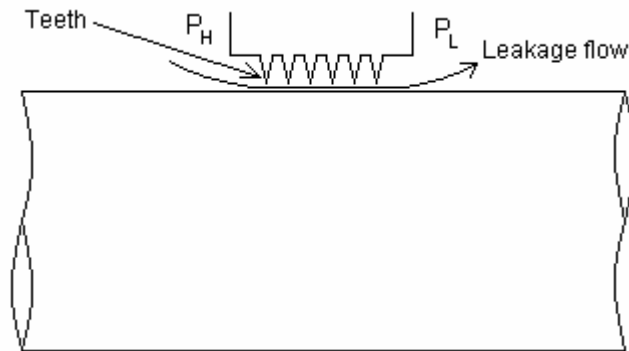
Figure 5: Labyrinth seal schematic.

Labyrinth seals are typically used as buffer seals in oil sealing applications. However, to prevent any contact between the teeth and the shaft surface in the case of radial excitations of the rotor, seal-rotor gap should be kept at the maximum distance of the rotor excitation calculated for landing and maneuver deflections in airplanes, and for vibrations and thermal dimensional changes during the startup and cooling of large turbine engines. As Foley et al. [17] reported, this gap is between 0.26 and 0.63mm (0.01in to 0.025 in), which is sufficient to let the leakage flows to cause efficiency losses or oil contamination problems in downstream sections. Additionally, experience has revealed that occasional large shaft excursions cause rubbing of the shaft to the

teeth of the labyrinth seal. This increases the leakage further since the gap becomes larger and since the turbulence inducing shape of the teeth changes [17]. As a consequence, the labyrinth seals are not sufficient in terms of oil leakage prevention.

Another solution to prevent oil leakage that has been tested and used in gas turbines has been the carbon circumferential seals, which are graphite contact seals that are aimed to prevent oil mist flow [4, 8]. Due to the lamellar atomic structure of the graphite, the rubbing life of these seals have been long, however Gorelev et al. [8] and Aksit et al. [4] reported that producing large seals from graphite leads to expensive production costs, and requires precise assembly. Gorelev et al. also informed that large rotor excitations also produce large gaps between the seal and the shaft surface, which causes the leakage increase with time.

Oil buffer seals like hydrogen cooled industrial generator applications involve sealing of oil instead of oil mist. Hydrodynamic oil rings have been employed for sealing of such continuous oil flows. However, it is crucial to maintain continuous leakage flow for continued seal performance. In absence of oil flow, oil rings can undergo excessive wear resulting in damaged seal and loss of performance [4].

Brush seals have been under development since early 90s [18], since they drop secondary leakage flows to a low, desirable level, and have proved to be quite durable [2, 3]. There have been several patents on the usage of brush seals as oil seals [19, 20, 21, 22]. It is reported that brush seals are used in aircraft engines for their compliance to rotor excursions and for their high level of sealing ability in both land-based and aircraft engines [8]. Brush seals have some hysteresis to follow the shaft surface after large transients of the rotor due to inter-bristle friction forces [9]. Additionally, long time in very high temperatures may cause deterioration which results in larger amount of leakage. However, this increased leakage also happens to a rubbed labyrinth seal [23]. Also, Chupp reports that the grooves found on the rotor due to the rubbing of labyrinth seals is much deeper than ever expected for the case of any brush seal [6]. Ferguson informed that through long-duration tests, the leakage of brush seal was still 5-10% of the same size labyrinth seals at the same test [24]. Also, Steinetz et al. reported that the engine experience has revealed improvements in engine performance and efficiency with the substitution of brush seals in the place of labyrinth seals [25]. According to the performance reports from some initial applications, the replacement of even one labyrinth seal by brush seals leaded to 0.4-1.9% total power output increase and these seals did not have any observable problem for 20000-40000 hour of operation [2]. Since

these compact sized seal easily fit to the space for labyrinth seals, they can also be adapted in the existing turbines for the improvement of their efficiency, so the retrofit ability is an additional appeal of these seals [6, 26, 27].

After numerous successful secondary flow cooling air applications oil and oil mist sealing applications are also considered [4]. Ingistov has been the first to report that properly designed brush seals can prevent the oil mist leakage better than labyrinth seals. Furthermore, studies by Aksit et al.[4], Braun et al. [28, 29], Carlile et al. [30] and Hendricks et al. [31] revealed that wet brush seals perform better as oil retained between the bristles further reduces porosity of the brush seals. Additionally, Shapiro et al. [5] reported that oil being a viscous material may provide additional damping of the rotor

2.2   Brush Seal Lifting Forces

Bristle tip forces are critical to know when finding equilibrium between hydrodynamic lift and reaction bristle forces. These forces are mainly hydrodynamic oil lift force, blow-down forces, frictional forces and beam bending forces. Some of the initial works on the application of brush seals for oil sealing by Ingistov [32], Bhate et al. [3] and Aksit et al. [4] has shown the effectiveness of the hydrodynamic lift on the bristle tip clearance through experimental evaluation. On the contrary, leakage reduces with the introduction of rotor speed air sealing applications due to increasing swirl ratio. As also reported by Wood and Jones [33], aerodynamic air lift force cannot overcome reaction forces on the bristles since air has a very low viscosity compared to oil. Therefore, analytical studies on brush seal air leakage studies are more concentrated on air penetration through the bristles instead of below the bristles.

Existing studies in the literature about the lift is generally on forces due to air flow. Hendricks et al. [34] worked on formulating bristle bending due to the aerodynamic forces through beam theory. There have been other studies [9, 35, 36, 37] to study pressure distribution and flows within the bristle pack through use of porous medium approach. The pressure distribution is used for evaluation of axial bending and blow-down forces. However, porous medium approach requires experimental data to determine the resistance coefficients in the formulation. Modi [38] and Sharatchandra et al. [39] studied aerodynamic lift on the bristles. Modi formulated this force using the porous medium approach. Sharatchandra et al. calculated the force numerically.

However, this work concentrates on estimating the bristle tip forces on the rotor surface rather than calculating lift clearance.

Since the oil lift on the bristles tips is very large compared to the lift force generated by air, considerable hydrodynamic lift occurs in oil sealing applications where main leakage occurs below the bristle tips instead of through the bristles. Since this leakage is directly related with the sealing performance of the brush seal, formulating the lift force is an important issue. Aksit et al. [4] provided an initial study for hydrodynamic lift of bristles using short bearing assumption based on the bearing and lubrication theory. However, there is no other published brush seal oil lift analysis. In an attempt to provide alternative solutions, this work also investigates long bearing and finite bearing solutions.

3   ANALYTICAL METHODOLOGY AND SOLUTION PROCEDURE

The approach used in this work is to model the lift forces on the bristles through hydrodynamic bearing theory. The motivation for this approach lies in the fact that due to the presence of bristle lay angle with rotor, each bristle tip forms small wedge acting like a small hydrodynamic bearing.

Layers of oil near the rotor surface is dragged by the rotating shaft, and pumped in to these small wedges thereby forming hydrodynamic lift pressure under each bristle. If the oil pressure distribution under the bristles is known, it will be possible to calculate the net lifting force by integrating the pressure over the bristle wedge area that the pressure acts on. Hydrodynamic pressure can be calculated through lubrication theory and Reynolds relations. The following sections will present derivation and adaptation of bearing equations to the bristle tip lift problem.
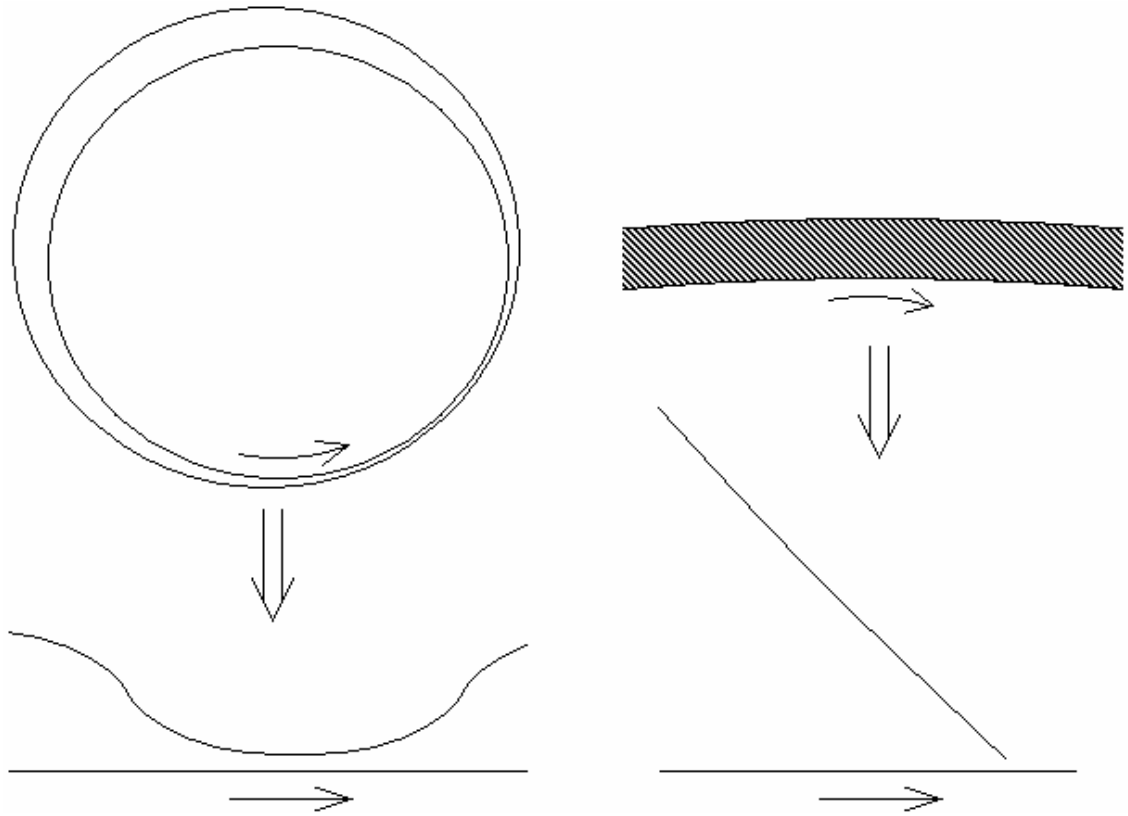
Figure 6: Wedge action of conformal bearing and brush seal.

3.1 Derivation of 2-D Reynolds Equation

The Reynolds Equation is a differential equation that determines the relation between the changes of pressure in different directions, clearance, viscosity and velocity. It is derived from the Navier-Stokes equations that are the general equations for determining the relation between density, viscosity, pressure, velocity, accelerations and gravitational accelerations of fluid particles. Since the Navier-Stokes equations are very complex to solve directly, there is a need to simplify and reduce them. As will be discussed in sections 3.1.2 and 3.1.4, simplification and reduction process involves order of magnitude analysis, and taking advantage of the thin film problem physics through the usage of boundary conditions and getting rid of inertia terms due to low Reynolds numbers.

3.1.1 Navier-Stokes Equations

The Navier-Stokes Equations consist of two sets of equations: Continuity and Momentum equations. The continuity equation captures the fact that no particle is generated or disappears within the system. The momentum equations are also called "Per volume momentum equations" since they are dimensionless in terms of volume.

Continuity:

$$\frac{\partial V_x}{\partial x} + \frac{\partial V_y}{\partial y} + \frac{\partial V_z}{\partial z} = 0$$

Momentum Equations:

$$\rho \left(\frac{\partial V_x}{\partial t} + V_x \frac{\partial V_x}{\partial x} + V_y \frac{\partial V_x}{\partial y} + V_z \frac{\partial V_x}{\partial z} \right) = -\frac{\partial P}{\partial x} + \mu \left(\frac{\partial^2 V_x}{\partial x^2} + \frac{\partial^2 V_x}{\partial y^2} + \frac{\partial^2 V_x}{\partial z^2} \right) - \rho g_x$$

$$\rho \left(\frac{\partial V_y}{\partial t} + V_x \frac{\partial V_y}{\partial x} + V_y \frac{\partial V_y}{\partial y} + V_z \frac{\partial V_y}{\partial z} \right) = -\frac{\partial P}{\partial y} + \mu \left(\frac{\partial^2 V_y}{\partial x^2} + \frac{\partial^2 V_y}{\partial y^2} + \frac{\partial^2 V_y}{\partial z^2} \right) - \rho g_y$$

$$\rho \left(\frac{\partial V_z}{\partial t} + V_x \frac{\partial V_z}{\partial x} + V_y \frac{\partial V_z}{\partial y} + V_z \frac{\partial V_z}{\partial z} \right) = -\frac{\partial P}{\partial z} + \mu \left(\frac{\partial^2 V_z}{\partial x^2} + \frac{\partial^2 V_z}{\partial y^2} + \frac{\partial^2 V_z}{\partial z^2} \right) - \rho g_z$$

3.1.2 Assumptions and reductions for 1-D Bearing Solution

1-D bearing means that the fluid in the bearing moves mainly in one direction. In cases where the length of the bearing in y direction (see Figure 7) is very long with respect to the length in x direction (or vice versa), this is a very plausible assumption. In applications where x or y dimensions are close in scale hydrodynamic lift force on the bristles will be calculated using 2-D bearing equations. A 1-D bearing equation defines a solution for 2-D bearing geometry where variations in x (or y) and z directions are considered. Similarly, 2-D bearing equation defines a solution full 3-D bearing geometry.
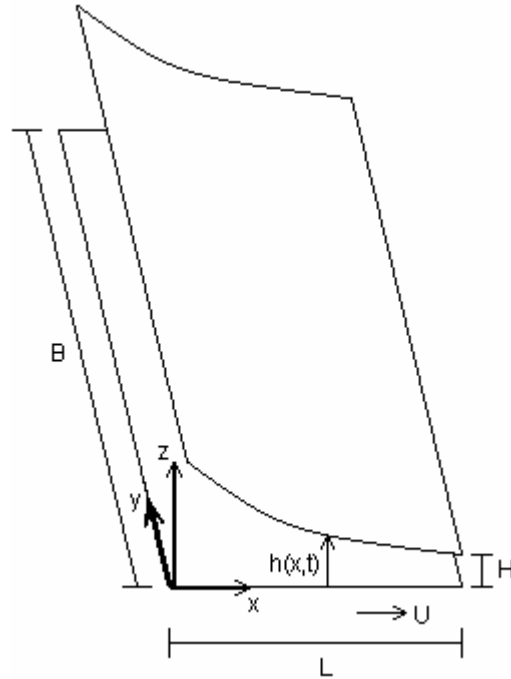
Figure 7: Schematic for 1-D bearing.

Consider the dimensional scales dictated by the geometry presented in Figure 7. Following dimensional scales govern the problem:

$$V_x \approx U$$

$$dx \approx L \qquad \frac{\partial}{\partial x} \approx \frac{1}{L}$$

$$dy \approx B \implies \frac{\partial}{\partial y} \approx \frac{1}{B}$$

$$dz \approx H$$

$$\frac{\partial}{\partial z} \approx \frac{1}{H}$$

Our problem involves:

1. Thin film   H<<L and H<<B   ($1/dz \gg 1/dx$, and $1/dz \gg 1/dy$)

2. 2-D Geometry, 1-D Bearing   B>>L ($1/dy \ll 1/dx$)

Now we can apply order of magnitude test to Navier-Stokes equations:

Continuity:

$$\frac{\partial V_x}{\partial x} + \frac{\partial V_y}{\partial y} + \frac{\partial V_z}{\partial z} = 0 \implies \frac{\partial V_x}{\partial x} + \frac{\partial V_z}{\partial z} = 0$$

$$\downarrow \qquad \downarrow \qquad \downarrow \qquad\qquad \downarrow$$

$$\approx \frac{U}{L} \qquad 0 \qquad \approx \frac{}{H} \qquad\qquad V_z \approx \frac{H}{L}U \approx \frac{H}{L}V_x$$

13

When the problem is solved in 2-D (1-D Bearing), (since y dependency is ignored) terms like V_y, $\dfrac{dV_y}{d...}$ and $\dfrac{d^2V_y}{d...^2}$ disappear, so the second momentum equation drops out. Therefore, momentum equations reduce as:

$$\frac{\partial V_x}{\partial y} = 0 \qquad\qquad dx \gg dz \quad \frac{\partial V_x}{\partial y} = 0 \text{ for all y} \quad g_x=0$$

$$\uparrow \qquad\qquad\qquad \uparrow \qquad \uparrow \qquad\qquad \uparrow$$

$$\rho\left(\frac{\partial V_x}{\partial t}+V_x\frac{\partial V_x}{\partial x}+V_y\frac{\partial V_x}{\partial y}+V_z\frac{\partial V_x}{\partial z}\right)=-\frac{\partial P}{\partial x}+\mu\left(\frac{\partial^2 V_x}{\partial x^2}+\frac{\partial^2 V_x}{\partial y^2}+\frac{\partial^2 V_x}{\partial z^2}\right)-\rho g_x$$

$V_z \ll V_x \Rightarrow$ Comparing with the equation above V_z's are cancelled.

$$\begin{array}{ccccccc} 0 & 0 & 0 & 0 & & 0 & 0 & 0 \\ \uparrow & \uparrow & \uparrow & \uparrow & & \uparrow & \uparrow & \uparrow \end{array}$$

$$\rho\left(\frac{\partial V_z}{\partial t}+V_x\frac{\partial V_z}{\partial x}+V_y\frac{\partial V_z}{\partial y}+V_z\frac{\partial V_z}{\partial z}\right)=-\frac{\partial P}{\partial z}+\mu\left(\frac{\partial^2 V_z}{\partial x^2}+\frac{\partial^2 V_z}{\partial y^2}+\frac{\partial^2 V_z}{\partial z^2}\right)-\rho g_z$$

$$\downarrow$$

Gravity neglected since it is ineffective when compared with other forces

Resulting equations:

Continuity:

$$\frac{\partial V_x}{\partial x}+\frac{\partial V_z}{\partial z}=0$$

X-momentum:

$$\rho\left(\frac{\partial V_x}{\partial t}+V_x\frac{\partial V_x}{\partial x}+V_z\frac{\partial V_x}{\partial z}\right)=-\frac{\partial P}{\partial x}+\mu\frac{\partial^2 V_x}{\partial z^2}$$

Z-momentum:

$$0=\frac{\partial P}{\partial z}$$

Since the fluid in the problem is oil, it is considered to be incompressible. To further simplify also consider constant effective viscosity. Making the equations nondimensional allows comparison of magnitude of each term leading further reductions. Consider the following scales for nondimensionalization:

$$x^* = \frac{x}{L} \approx 1$$

$$z^* = \frac{z}{H} \approx 1$$

$$V_x^* = \frac{V_x}{U} \approx 1$$

$$V_z^* = \frac{V_z}{H} \approx \frac{1}{H}\frac{H}{L}U \approx \frac{U}{L}V_x^*$$

$$t^* = \frac{tU}{L} \approx 1$$

$$P^* = \frac{(P - P_{atm})H^2}{\mu U L} \approx 1$$

Applying the scale factors, the nondimensional x-momentum becomes:

$$\rho\frac{U^2}{L}\left(\frac{\partial V_x^*}{\partial t^*} + V_x^*\frac{\partial V_x^*}{\partial x^*} + V_x^*\frac{\partial V_x^*}{\partial z^*}\right) = -\frac{\mu U}{H^2}\frac{\partial P^*}{\partial x^*} + \frac{\mu U}{H^2}\frac{\partial^2 V_x^*}{\partial z^{*2}}$$

Grouping some terms Reynolds number becomes:

$$\mathrm{Re}^* = \left(\frac{\rho U H}{\mu}\right)\frac{H}{L} = \mathrm{Re}\frac{H}{L}$$

Using typical oil bearing parameter values:

$$\rho = 900\frac{kg}{m^3}$$

$$H = 50\,\mu m$$

$$\mu = 0.025 Pa - s$$

$$U = 10\frac{m}{s}$$

$$L = 0.05 m$$

Reynolds number becomes:

$$\mathrm{Re}^* = 0.018 \approx 10^{-2}.$$

$$\mathrm{Re}^*\left(\frac{\partial V_x^*}{\partial t^*} + V_x^*\frac{\partial V_x^*}{\partial x^*} + V_x^*\frac{\partial V_x^*}{\partial z^*}\right) = -\frac{\partial P^*}{\partial x^*} + \frac{\partial^2 V_x^*}{\partial z^{*2}}$$

$$\downarrow \qquad\qquad \downarrow \qquad\qquad \downarrow \qquad \downarrow$$

$$\approx 10^{-2} \qquad\qquad \approx 1 \qquad\qquad \approx 1 \qquad \approx 1$$

Therefore, inertia terms on the left side drop compared to pressure and viscous terms.

3.1.3 Application of boundary conditions and calculations for 1-D Bearing

After all cancellations Navier Stokes equations reduce to:

Mass balance:

$$\frac{\partial V_x}{\partial x} + \frac{\partial V_z}{\partial z} = 0$$

Force balance:

$$0 = -\frac{\partial P}{\partial x} + \mu \frac{\partial^2 V_x}{\partial z^2} \qquad\qquad 0 = \frac{\partial P}{\partial z}.$$

Apply boundary conditions to solve:

$$z = 0 \Rightarrow V_x = U, \ V_z = 0$$

$$z = h(x,t) \Rightarrow V_x = 0, \quad V_z = \frac{\partial h}{\partial t}$$

$$\frac{\partial^2 V_x}{\partial z^2} = \frac{1}{\mu}\frac{\partial P}{\partial x} \implies \frac{\partial V_x}{\partial z} = \frac{1}{\mu}\frac{\partial P}{\partial x}z + c_1(x,t)$$

$$V_x = \frac{1}{2\mu}\frac{\partial P}{\partial x}z^2 + c_1(x,t)z + c_2(x,t)$$

$$z = 0 \Rightarrow V_x = U = c_2(x,t) \Rightarrow c_2 = U$$

$$z = h \Rightarrow 0 = \frac{1}{2\mu}\frac{\partial P}{\partial x}h^2 + c_1 h + U \Rightarrow c_1 = -\frac{1}{2\mu}\frac{\partial P}{\partial x}h - \frac{U}{h}$$

$$V_x = \frac{1}{2\mu}\frac{\partial P}{\partial x}\left(z^2 - zh\right) + U\left(1 - \frac{z}{h}\right)$$

$$\int_0^h \left(\frac{\partial V_x}{\partial x} + \frac{\partial V_z}{\partial z}\right)dz = 0$$

$$\int_0^h \frac{\partial V_x}{\partial x}dz + \int_0^h \frac{\partial V_z}{\partial z}dz = 0$$

$$\downarrow$$

$$V_z(z = h) - V_z(z = 0)$$

$$\downarrow \qquad\quad \downarrow$$

$$\frac{\partial h}{\partial t} \qquad\quad 0$$

Apply Leibnitz Rule:

$$\frac{\partial}{\partial x}\int_{a(x)}^{b(x)} f(x,z)dz = \int_{a(x)}^{b(x)}\frac{\partial f}{\partial x}dz + \frac{\partial b}{\partial x}f(x,b) - \frac{\partial a}{\partial x}f(x,a)$$

$$\Downarrow$$

$$\frac{\partial}{\partial x}\int_{0}^{h(x,t)} V_x dz = \int_{0}^{h}\frac{\partial V_x}{\partial x}dz + \frac{\partial h}{\partial x}V_x(x,z=h) - \frac{\partial(0)}{\partial x}V_x(x,z=0)$$

$$\downarrow \qquad\qquad \downarrow$$

$$0 \qquad\qquad 0$$

$$\frac{\partial}{\partial x}\int_{0}^{h(x,t)} V_x dz = \int_{0}^{h}\frac{\partial V_x}{\partial x}dz$$

$$\int_{0}^{h} V_x dz = \frac{1}{2\mu}\frac{\partial P}{\partial x}\left(\frac{z^3}{3}-\frac{z^2}{2}h\right)\Bigg|_0^h + U\left(z-\frac{z^2}{2h}\right)\Bigg|_0^h = -\frac{h^3}{12\mu}\frac{\partial P}{\partial x}+\frac{Uh}{2}$$

$$\int_{0}^{h}\frac{\partial V_x}{\partial x}dz = \frac{\partial}{\partial x}\left(-\frac{h^3}{12\mu}\frac{\partial P}{\partial x}+\frac{Uh}{2}\right)$$

$$\int_{0}^{h}\frac{\partial V_x}{\partial x}dz + \frac{\partial h}{\partial t}=0 \Rightarrow \frac{\partial}{\partial x}\left(-\frac{h^3}{12\mu}\frac{\partial P}{\partial x}+\frac{Uh}{2}\right)+\frac{\partial h}{\partial t}=0$$

$$\frac{\partial}{\partial x}\left(\frac{h^3}{\mu}\frac{\partial P}{\partial x}\right) = 6U\frac{\partial h}{\partial x}+12\frac{\partial h}{\partial t}$$

3.1.4   Assumptions and reductions for 2-D Bearing
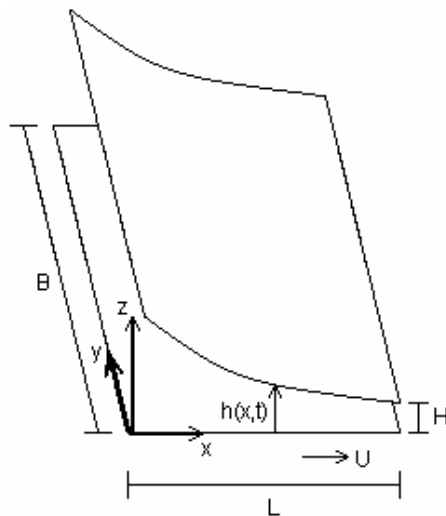
Figure 8: Schematic for 2-D bearing.

Consider the dimensional scales dictated by the geometry presented in Figure 8. Following dimensional scales govern the problem:

$$V_x \approx U$$

$$dx \approx L \quad \frac{\partial}{\partial x} \approx \frac{1}{L}$$

$$dy \approx B \Rightarrow \frac{\partial}{\partial y} \approx \frac{1}{B}$$

$$dz \approx H$$

$$\frac{\partial}{\partial z} \approx \frac{1}{H}$$

Our problem involves thin film geometry, H<<L and H<<B, leading to ($1/dz \gg 1/dx$, and $1/dz \gg 1/dy$). Applying order of magnitude test to Navier-Stokes equations:

Continuity:

$$\frac{\partial V_x}{\partial x} + \frac{\partial V_y}{\partial y} + \frac{\partial V_z}{\partial z} = 0$$

$$V_z \approx \frac{H}{L} U \approx \frac{H}{L} V_x$$

Order of magnitude for V_y is an unknown. Therefore, no cancellation could be done in the continuity equation.

Momentum Equations:

$$dx \gg dz \quad dy \gg dz \qquad g_x = 0$$
$$\uparrow \qquad \uparrow \qquad \uparrow$$

$$\rho\left(\frac{\partial V_x}{\partial t} + V_x \frac{\partial V_x}{\partial x} + V_y \frac{\partial V_x}{\partial y} + V_z \frac{\partial V_x}{\partial z}\right) = -\frac{\partial P}{\partial x} + \mu\left(\frac{\partial^2 V_x}{\partial x^2} + \frac{\partial^2 V_x}{\partial y^2} + \frac{\partial^2 V_x}{\partial z^2}\right) - \rho g_x$$

$$dx \gg dz \quad dy \gg dz \qquad g_y = 0$$
$$\uparrow \qquad \uparrow \qquad \uparrow$$

$$\rho\left(\frac{\partial V_y}{\partial t} + V_x \frac{\partial V_y}{\partial x} + V_y \frac{\partial V_y}{\partial y} + V_z \frac{\partial V_y}{\partial z}\right) = -\frac{\partial P}{\partial y} + \mu\left(\frac{\partial^2 V_y}{\partial x^2} + \frac{\partial^2 V_y}{\partial y^2} + \frac{\partial^2 V_y}{\partial z^2}\right) - \rho g_y$$

$$V_z \ll V_x \text{ and } V_z \ll V_y$$

Therefore V_z and V_z^2 terms drop.

$$
\begin{array}{ccccccc}
0 & 0 & 0 & 0 & \quad & 0 & 0 & 0 \\
\uparrow & \uparrow & \uparrow & \uparrow & \quad & \uparrow & \uparrow & \uparrow
\end{array}
$$

$$
\rho\left(\frac{\partial V_z}{\partial t}+V_x\frac{\partial V_z}{\partial x}+V_y\frac{\partial V_z}{\partial y}+V_z\frac{\partial V_z}{\partial z}\right)=-\frac{\partial P}{\partial z}+\mu\left(\frac{\partial^2 V_z}{\partial x^2}+\frac{\partial^2 V_z}{\partial y^2}+\frac{\partial^2 V_z}{\partial z^2}\right)-\rho g_z
$$

$$\downarrow$$

Gravity neglected (gravity acting on fluid particles are very small compared to other forces)

Similar to the process applied in 1-D bearings in the section 3.1.2 after nondimensionalization and checking for Reynolds numbers, left side inertial terms drop compared to the pressure and viscous terms.

Therefore, Navier Stokes equations reduce to:

Continuity:

$$
\frac{\partial V_x}{\partial x}+\frac{\partial V_y}{\partial y}+\frac{\partial V_z}{\partial z}=0
$$

X-momentum:

$$
0=-\frac{\partial P}{\partial x}+\mu\frac{\partial^2 V_x}{\partial z^2}
$$

Y-momentum:

$$
0=-\frac{\partial P}{\partial y}+\mu\frac{\partial^2 V_y}{\partial z^2}
$$

Z-momentum:

$$
0=\frac{\partial P}{\partial z}
$$

3.1.5   Application of boundary conditions and calculations for 2-D Bearing

The equations after all cancellations become:

Mass balance:

$$
\frac{\partial V_x}{\partial x}+\frac{\partial V_y}{\partial y}+\frac{\partial V_z}{\partial z}=0
$$

Force balance:

$$0 = -\frac{\partial P}{\partial x} + \mu \frac{\partial^2 V_x}{\partial z^2} \qquad 0 = -\frac{\partial P}{\partial y} + \mu \frac{\partial^2 V_y}{\partial z^2} \qquad 0 = \frac{\partial P}{\partial z}$$

Apply boundary conditions to solve:

$$z = 0 \Rightarrow V_x = U,\ V_y = 0, \qquad V_z = 0$$

$$z = h(x,t) \Rightarrow V_x = 0, \quad V_y = 0, \qquad V_z = \frac{\partial h}{\partial t}$$

$$\frac{\partial^2 V_x}{\partial z^2} = \frac{1}{\mu}\frac{\partial P}{\partial x} \Rightarrow \frac{\partial V_x}{\partial z} = \frac{1}{\mu}\frac{\partial P}{\partial x} z + c_1(x,t) \Rightarrow V_x = \frac{1}{2\mu}\frac{\partial P}{\partial x} z^2 + c_1(x,t) z + c_2(x,t)$$

$$z = 0 \Rightarrow V_x = U = c_2(x,t) \Rightarrow c_2 = U$$

$$z = h \Rightarrow 0 = \frac{1}{2\mu}\frac{\partial P}{\partial x} h^2 + c_1 h + U \Rightarrow c_1 = -\frac{1}{2\mu}\frac{\partial P}{\partial x} h - \frac{U}{h}$$

$$V_x = \frac{1}{2\mu}\frac{\partial P}{\partial x}\left(z^2 - zh\right) + U\left(1 - \frac{z}{h}\right)$$

Therefore, x-component of the velocity profile contains both pressure and velocity driven terms.

$$\frac{\partial^2 V_y}{\partial z^2} = \frac{1}{\mu}\frac{\partial P}{\partial y} \Rightarrow \frac{\partial V_y}{\partial z} = \frac{1}{\mu}\frac{\partial P}{\partial y} z + c_1(x,t) \Rightarrow V_y = \frac{1}{2\mu}\frac{\partial P}{\partial y} z^2 + c_1(x,t) z + c_2(x,t)$$

$$z = 0 \Rightarrow V_y = 0 = c_2(x,t) \Rightarrow c_2 = 0$$

$$z = h \Rightarrow 0 = \frac{1}{2\mu}\frac{\partial P}{\partial y} h^2 + c_1 h \Rightarrow c_1 = -\frac{1}{2\mu}\frac{\partial P}{\partial y} h$$

$$V_y = \frac{1}{2\mu}\frac{\partial P}{\partial y}\left(z^2 - zh\right)$$

Therefore, y-component of the velocity profile contains only pressure driven terms as expected.

$$\int_0^h \left(\frac{\partial V_x}{\partial x} + \frac{\partial V_y}{\partial y} + \frac{\partial V_z}{\partial z}\right) dz = 0$$

$$\int_0^h \frac{\partial V_x}{\partial x} dz + \int_0^h \frac{\partial V_y}{\partial y} dz + \int_0^h \frac{\partial V_z}{\partial z} dz = 0$$

$$\downarrow$$

$$V_z(z = h) - V_z(z = 0)$$

$$\downarrow \qquad \downarrow$$

$$\frac{\partial h}{\partial t} \qquad 0$$

According to the Leibnitz Rule presented in section 3.1.3:

$$\frac{\partial}{\partial x} \int_0^{h(x,t)} V_x dz = \int_0^h \frac{\partial V_x}{\partial x} dz + \frac{\partial h}{\partial x} V_x(x, z = h) - \frac{\partial(0)}{\partial x} V_x(x, z = 0)$$

$$\downarrow \qquad \downarrow$$

$$0 \qquad 0$$

$$\frac{\partial}{\partial x} \int_0^{h(x,t)} V_x dz = \int_0^h \frac{\partial V_x}{\partial x} dz$$

$$\int_0^h V_x dz = \frac{1}{2\mu} \frac{\partial P}{\partial x} \left(\frac{z^3}{3} - \frac{z^2}{2} h \right) \Bigg|_0^h + U \left(z - \frac{z^2}{2h} \right) \Bigg|_0^h = -\frac{h^3}{12\mu} \frac{\partial P}{\partial x} + \frac{Uh}{2}$$

$$\int_0^h \frac{\partial V_x}{\partial x} dz = \frac{\partial}{\partial x} \left(-\frac{h^3}{12\mu} \frac{\partial P}{\partial x} + \frac{Uh}{2} \right)$$

$$\frac{\partial}{\partial y} \int_0^{h(x,t)} V_y dz = \int_0^h \frac{\partial V_y}{\partial y} dz + \frac{\partial h}{\partial y} V_y(y, z = h) - \frac{\partial(0)}{\partial y} V_y(y, z = 0)$$

$$\downarrow \qquad \downarrow$$

$$0 \qquad 0$$

$$\frac{\partial}{\partial y} \int_0^{h(x,t)} V_y dz = \int_0^h \frac{\partial V_y}{\partial y} dz$$

$$\int_0^h V_y dz = \frac{1}{2\mu} \frac{\partial P}{\partial y} \left(\frac{z^3}{3} - \frac{z^2}{2} h \right) \Bigg|_0^h = -\frac{h^3}{12\mu} \frac{\partial P}{\partial y}$$

$$\int_0^h \frac{\partial V_y}{\partial y} dz = \frac{\partial}{\partial y} \left(-\frac{h^3}{12\mu} \frac{\partial P}{\partial y} \right)$$

$$\int_0^h \frac{\partial V_x}{\partial x} dz + \int_0^h \frac{\partial V_y}{\partial y} dz + \int_0^h \frac{\partial V_z}{\partial z} dz = 0$$

21

$$\int_0^h \frac{\partial V_x}{\partial x}dz + \int_0^h \frac{\partial V_x}{\partial x}dz + \frac{\partial h}{\partial t} = 0 \Rightarrow \frac{\partial}{\partial x}\left(-\frac{h^3}{12\mu}\frac{\partial P}{\partial x} + \frac{Uh}{2}\right) + \frac{\partial}{\partial y}\left(-\frac{h^3}{12\mu}\frac{\partial P}{\partial y}\right) + \frac{\partial h}{\partial t} = 0$$

Since μ is assumed to be constant (effective viscosity considered):

$$\frac{\partial}{\partial x}\left(h^3 \frac{\partial P}{\partial x}\right) + \frac{\partial}{\partial y}\left(h^3 \frac{\partial P}{\partial y}\right) = 6\mu U \frac{\partial h}{\partial x} + 12\mu \frac{\partial h}{\partial t}$$

This equation is the 2-D Reynolds equation for bearings. In this equation the term $12\mu\dfrac{dh}{dt}$ represents time dependent transients. For steady state analysis this term will drop. As a result, general Reynolds equation becomes:

$$\frac{\partial}{\partial x}\left(h^3 \frac{\partial P}{\partial x}\right) + \frac{\partial}{\partial y}\left(h^3 \frac{\partial P}{\partial y}\right) = 6\mu U \frac{\partial h}{\partial x}$$

3.2   Short Bearing Solution

Aksit et al. [40] has published a study on the hydrodynamic oil lift of brush seal bristles based on short bearing assumption. This work is primarily based on the theory that each bristle in the pack behaves individually. As a result, the assumptions in the formulation are made with the idea that there is only one bristle in the space.

3.2.1   Assumptions

For a general 2-D steady bearing with constant viscosity and incompressible oil film, the Reynolds equation for hydrodynamic bearings has been derived above as:

$$\frac{\partial}{\partial x}\left(h^3 \frac{\partial P}{\partial x}\right) + \frac{\partial}{\partial y}\left(h^3 \frac{\partial P}{\partial y}\right) = 6\mu U \frac{\partial h}{\partial x}$$

Consider the bristle shown in Figure 9 with its tip is placed above the origin and bristle extends in the negative x direction.
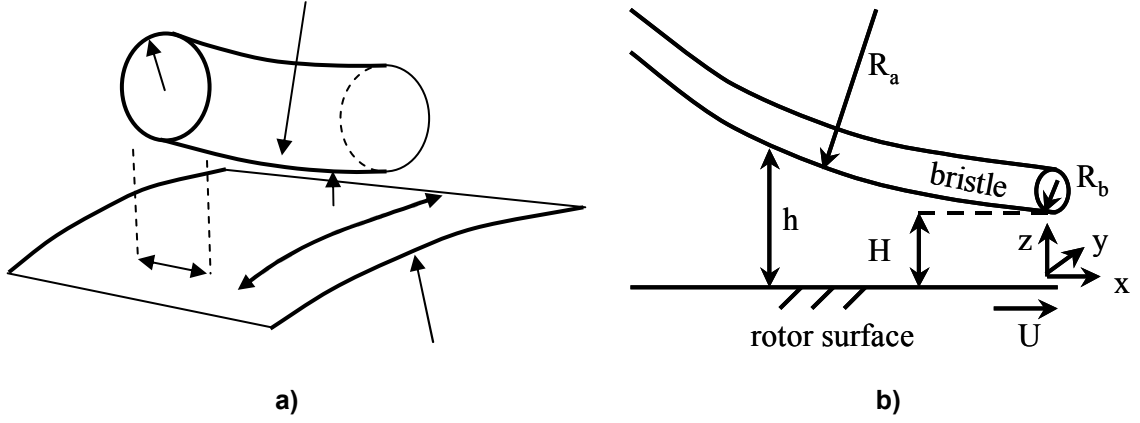
Figure 9: Bristle geometry: a) actual, b) simplified [40].

In this formulation, the boundary conditions for the pressure in a typical bearing can be stated as:

$$P(y \to \infty) = P_a, \text{ and } \left.\frac{\partial P}{\partial y}\right|_{y=0} = 0 \text{ (pressure is symmetric with respect to x axis),}$$

where P_a is the ambient pressure. It can be considered as atmospheric pressure in the ventilated bearings or the sump pressure in the pressurized bearings. Since the pressure arises due to the wedge action, the clearance between the bristle surface and the rotor surface is crucial. To solve Reynolds equation, we need to define clearance, h in terms of x,y,z. Hertzian contact formulation for spacing between two cylinders with inclined axes is utilized to model the clearance as follows:

$$h = H + \frac{x^2}{2R_a} + \frac{y^2}{2R_b} \text{ [48]}$$

In this formulation, H is the clearance of the bristle tip from the rotor surface. R_a is the equivalent bristle bending curvature that is defined as:

$$\frac{1}{R_a} = \frac{1}{R_A} + \frac{1}{R_R} \text{ [48]}$$

Since both the bristle has a bending and the surface of the rotor is round in x direction, R_a is formulated in a way to combine both radia as an equivalent curvature. In this formulation variation in y direction is dictated by R_b, and in the x direction by R_a. Noting that:

$$R_a \gg R_b$$

$$\frac{\partial}{\partial x} \approx \frac{1}{\sqrt{HR_a}} << \frac{\partial}{\partial y} \approx \frac{1}{\sqrt{HR_b}}$$

As R_a is very large compared to R_b, bearing width is very short compared to the bearing length. This is why this solution is called short bearing solution. The large scale difference further simplifies the 2-D bearing equation as:

$$\frac{\partial}{\partial y}\left(h^3 \frac{\partial P}{\partial y} \right) = 6\mu U \frac{\partial h}{\partial x}$$

3.2.2 Solution procedure

The equation $h = H + \frac{x^2}{2R_a} + \frac{y^2}{2R_b}$ leads to the equation $\frac{dh}{dx} = \frac{x}{R_a}$ when the derivative is taken. When this new relation is applied to the simplified version of the 2-D bearing equation, the equation becomes:

$$\frac{d}{dy}\left[h^3 \frac{\partial P}{\partial y} \right] = 6\mu U \frac{x}{R_a}$$

Taking the integral per dy, the equation becomes:

$$h^3 \frac{\partial P}{\partial y} = 6\mu U \frac{x}{R_a} y + c_1$$

Apply the symmetry boundary condition, i.e., pressure profile is symmetry about x axis (bristle center):

$$\left. \frac{\partial P}{\partial y} \right|_{y=0} = 0 \Rightarrow c_1 = 0$$

Rearranging, the equation becomes:

$$\frac{\partial P}{\partial y} = \frac{6\mu U}{R_a} \frac{xy}{h^3} = \frac{6\mu U}{R_a} \frac{xy}{\left(H + \frac{x^2}{2R_a} + \frac{y^2}{2R_b} \right)^3}$$

Integrate again to get oil lift pressure as

$$P = \int \frac{\partial P}{\partial y} dy + c_2(x) = \frac{6\mu U x}{R_a} \left[-\frac{R_b}{2} \frac{1}{\left(H + \frac{x^2}{2R_a} + \frac{y^2}{2R_b} \right)^2} \right] + c_2(x)$$

24

To find c_2, the boundary condition $P(y \to \infty) = P_a$ is used. As neighboring bristles are ignored, this helps simplify the solution to obtain integration constant as:

$$c_2 = P_a \Rightarrow P - P_a = -\frac{3\mu U x R_b}{R_a}\frac{1}{h^2} = -3\mu\frac{U}{h}\frac{R_b}{h}\frac{x}{R_a}$$

To find the lift force due to the oil pressure driven by the wedge action, the pressure should be integrated over the bristle area:

$$W = 2\int_{-\infty}^{0}\int_{0}^{\infty}(P - P_a)\,dxdy$$

Noting the symmetry about the x axis, y-integration is performed only on the one side of the bristle. Then the result is multiplied by two. Substituting in the P-P$_a$ in to the force equation leads to:

$$W = \frac{6\mu U R_b}{R_a}\int_{0}^{\infty}\int_{0}^{\infty}\frac{xdxdy}{\left(H + \dfrac{x^2}{2R_a} + \dfrac{y^2}{2R_b}\right)^2} = \frac{6\mu U R_b}{R_a}\pi R_a\sqrt{\frac{R_b}{2H}}$$

which is briefly:

$$W = \frac{6\pi}{\sqrt{2}}\mu U R_b\sqrt{\frac{R_b}{H}}$$

During operation, this hydrodynamic lift force will be balanced by the bristle tip reaction forces generated by beam deflection, blow down etc. If such forces are known, hydrodynamic lift clearance can be calculated taking advantage of this equilibrium. Therefore, H can be calculated as:

$$H = 18\pi^2\mu^2 R_b^{\,3}\left(\frac{U}{W}\right)^2$$

3.3   Long Bearing Solution

Short bearing formulation presented in the preceding section assumes that oil pumped by the shaft rotation fully penetrates through the brush pack developing lift pressure over the entire bristle surface. However, it is obvious that the bristles in the brush seals become tightly packed as the pressure difference between the high and low pressure zones increases [9]. As a result, penetration of the oil pumped by the shaft

rotation will be somewhat limited. In reality, amount of bristle tip area exposed to the hydrodynamic lift pressure will vary depending on how tightly the bristles are packed under the operating conditions for a given seal design. Contrary to the short bearing assumption, in the long bearing approach it is assumed that the bristles are so tightly packed that only the small tip region of each bristle is exposed to the pumped oil pressure. As a result, the x distance (L in Figure 8) of the pressure zone becomes small compared to the y distance (B in Figure 8). In the short bearing solution of the problem in section 3.2.1, the simplifications were made according to the consideration as $\frac{d}{dx} << \frac{d}{dy}$, because bearing width B was small (short) compared to the x scale L. For the long bearing approach the opposite is true. That is:

$$\frac{d}{dy} << \frac{d}{dx}$$

Therefore y-terms drop from the left side, reducing the 2-D Reynolds equation derived in Section 3.1.5 to:

$$\frac{d}{dx}\left(h^3 \frac{dP}{dx} \right) = 6\mu U \frac{dh}{dx}$$

3.3.1   Assumptions

There are some plausible assumptions that can simplify the solution of the problem. The first one is that the bristles are considered as straight cylinders that have cant angles with the normal of the rotor surface as shown in the Figure 10. As reported by Aksit et al. [40] hydrodynamic lift causes less than 50μm deflection (bristle tip clearance). Considering also the fact that only the very tip of the bristles are evaluated, changes in bristle lay angle are neglected.
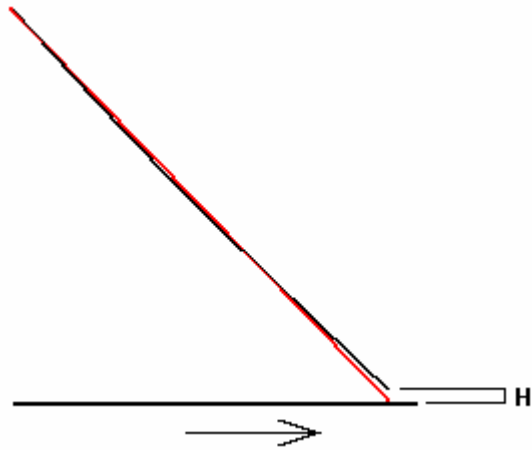
Figure 10: Deviations from bristle cant angle are neglected due to small deflections.

The second assumption is that the bristle tip surface is considered parallel to the rotor surface as illustrated in the Figure 11. When a brush seal is produced, the tips of the bristles are cut using a wire EDM (Electro-Discharge Machining) process. This circumferential cutting generates bristle tips parallel to the rotor surface to a certain degree. Additionally, most seal wear happens during early transients conforming the bristle tip surfaces to the rotor. Since the bending of the bristles is very small, even after the oil lift, the bristle tip surface and the rotor surface remain nearly parallel.
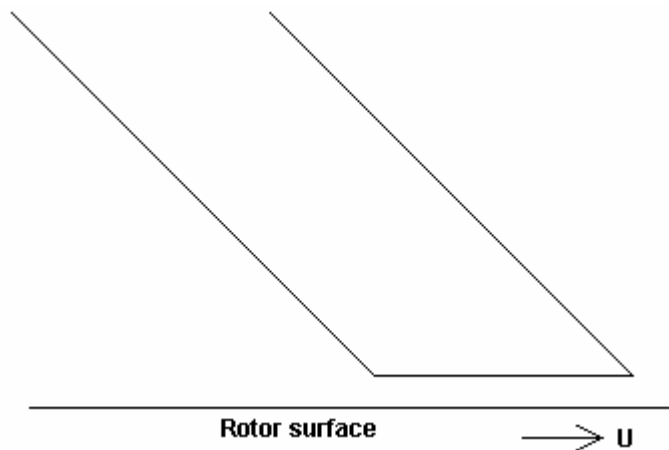

Figure 11: Bristle tips assumed to remain parallel to the rotor surface.

The third assumption is that (as illustrated in Figure 12) bristles are so tightly packed that only a small circumferential gap between the bristles is available for hydrodynamic lift pressure to develop.
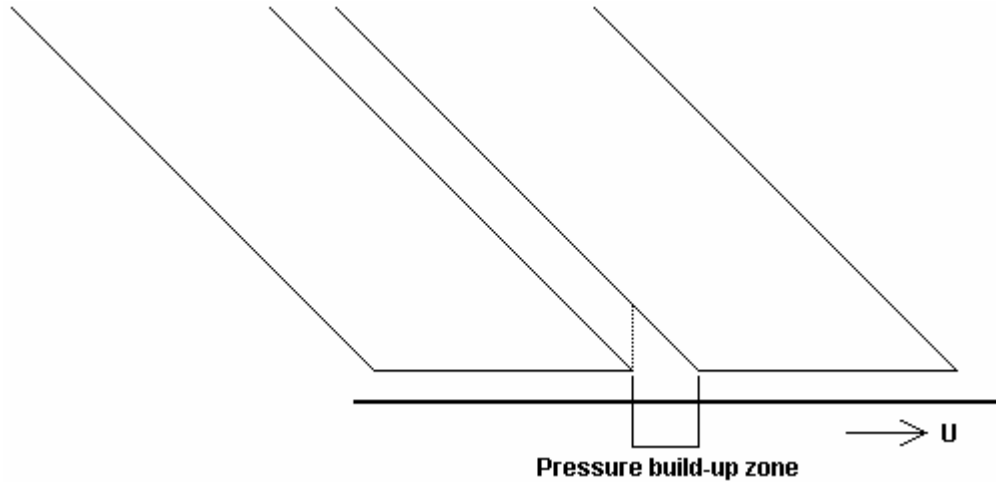
Figure 12: 2-D sketch of pressure build-up zone between the bristles.

Finally, hydrodynamic lift force is assumed to develop only in the wedge section and any small contributions (if any) from the bristle footprint region is neglected. This assumption is similar to the common procedure called as "Half Sommerfeld" boundary condition applied in common journal bearing solutions. Therefore, edges of the subsequent bristle footprints form the integration limits. Figure 13 illustrates how values for the "LimitLow" and "LimitHigh" for a y value are calculated.
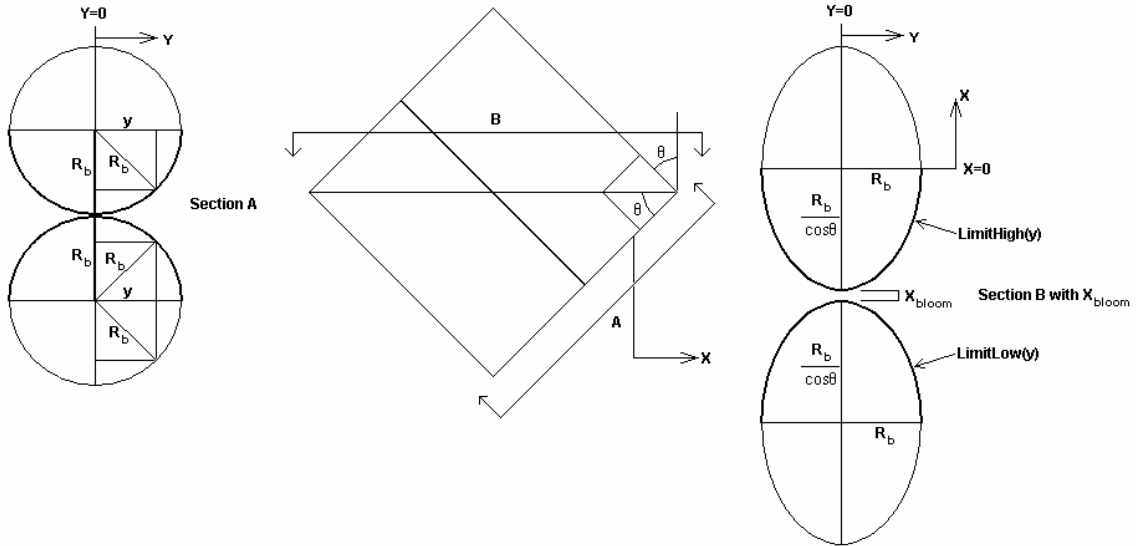
Figure 13: Footprint of the bristles.

From the geometry,

$$LimitLow = \frac{-2R_b + \sqrt{R_b{}^2 - y^2}}{\cos\theta} - X_{bloom}$$

$$\text{LimitHigh} = \frac{-\sqrt{R_b^2 - y^2}}{\cos\theta}$$

X_{bloom} is the inter-bristle distance in the x direction. Aksit [7] reported this distance to be around $X_{\text{bloom}} = 0.05 \dfrac{2R_b}{\cos\theta}$.

Because bristles have cant angle θ with rotor, variation of radial distance between rotor and inclined bristle surface (clearance) can be formulated as:

$$h = H - \frac{\sqrt{R_b^2 - y^2}}{\sin\theta} - \frac{1}{\tan\theta} x$$

Figure 14 illustrates how this formula is obtained. 3-D representation of the inter-bristle hydrodynamic bearing geometry is also illustrated in Figure 15.
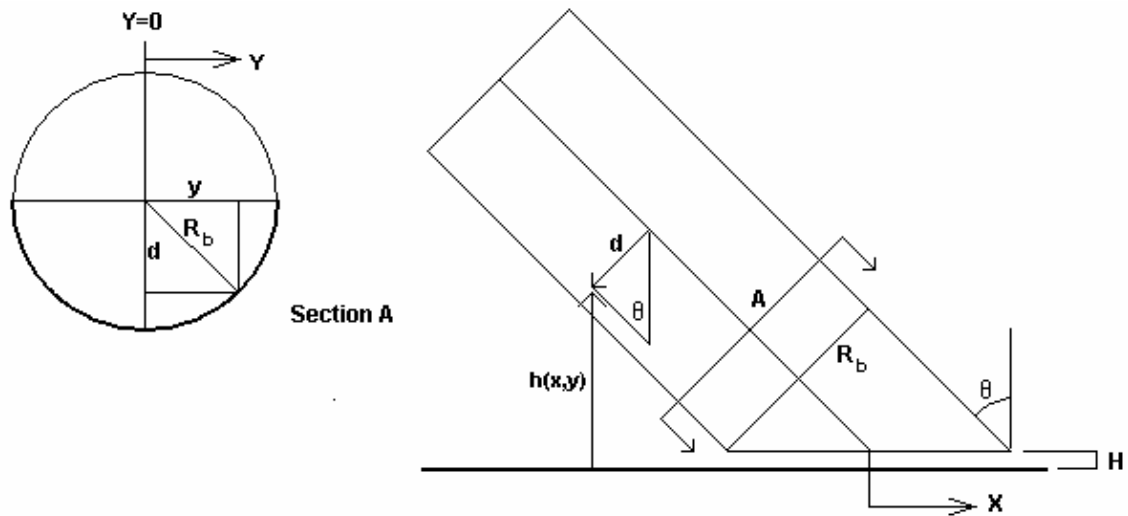
Figure 14: Height under the bristle.
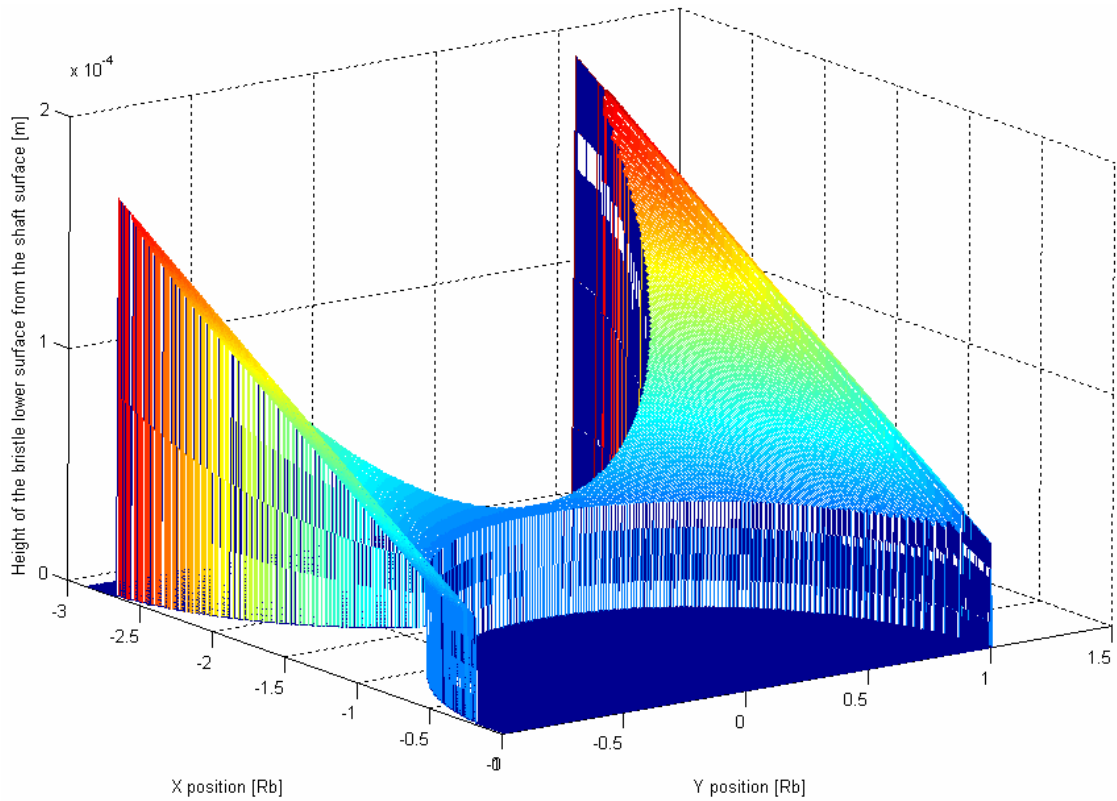
Figure 15: Bristle tip area exposed to the oil lift.

3.3.2   Solution procedure

Let's start with the long bearing version of the Reynolds equation derived in section 3.3.

$$\frac{\partial}{\partial x}\left(\frac{\rho h^3}{\mu}\frac{\partial P}{\partial x}\right) = 6\,U\frac{\partial(\rho h)}{\partial x}$$

Since this paper does not deal with shear heating in the bristle pack, a constant effective temperature is considered. Therefore, ρ (viscosity) is constant.

$$\frac{\partial}{\partial x}\left(h^3\frac{\partial P}{\partial x}\right) = 6\mu\,U\frac{\partial h}{\partial x}$$

Integrate once to get

$$h^3 \frac{\partial P}{\partial x} = 6\mu U h + C_1$$

$$C_1 = -h_m 6\mu U \qquad \text{(where } h_m \text{ is the h value at } \partial P/\partial x = 0)$$

$$\frac{\partial P}{\partial x} = 6\mu U \left(\frac{h - h_m}{h^3} \right)$$

⇩ Integrating again with respect to x

$$P = 6\mu U \int_{LimitLow}^{x} \frac{h(x) - h_m}{h^3(x)} dx + C_2$$

We need to find h_m and c_2:

$P = P_a$ @ x = LimitHigh, and x = LimitLow

$$P\Big|_{LimitHigh} - P\Big|_{LimitLow} = 0 = 6\mu U \left(\int_{LimitLow}^{LimitHigh} \frac{dx}{h^2(x)} - h_m \int_{LimitLow}^{LimitHigh} \frac{dx}{h^3(x)} \right)$$

$$h_m = \frac{\int_{LimitLow}^{LimitHigh} \frac{dx}{h^2(x)}}{\int_{LimitLow}^{LimitHigh} \frac{dx}{h^3(x)}}$$

Now plug in the h function defined before

$$h = H - \frac{\sqrt{R_b^2 - y^2}}{\sin \theta} - \frac{1}{\tan \theta} x$$

|----------a----------|----b-----|

$$a = H - \frac{\sqrt{R_b{}^2 - y^2}}{\sin \theta}$$

$$b = -\frac{1}{\tan \theta}$$

$$\int \frac{dx}{(a+bx)^2} = -\frac{1}{-\frac{1}{\tan \theta}(a+bx)} = \frac{\tan \theta}{a+bx}$$

$$\int \frac{dx}{(a+bx)^3} = -\frac{1}{2\frac{-1}{\tan \theta}(a+bx)^2} = \frac{\tan \theta}{2(a+bx)^2}$$

$$h_m = \frac{\tan \theta \left(\frac{1}{a+bLimitHigh} - \frac{1}{a+bLimitLow} \right)}{\frac{\tan \theta}{2} \left(\frac{1}{(a+bLimitHigh)^2} - \frac{1}{(a+bLimitLow)^2} \right)}$$

$$h_m = \frac{2}{\left(\frac{1}{a+bLimitHigh} + \frac{1}{a+bLimitLow} \right)}$$

$$h_m = \frac{2(a+bLimitHigh)(a+bLimitLow)}{2a+b(LimitHigh+LimitLow)}$$

$$P\big|_{LimitLow} = P\big|_{LimitHigh} = P_a = C_2$$

$$P - P_a = 6\mu\, U \left(\int_{LimitLow}^{x} \frac{dx}{h^2(x)} - h_m \int_{LimitLow}^{x} \frac{dx}{h^3(x)} \right)$$

$$P - P_a = 6\mu\, U \tan \theta \left(\frac{\frac{1}{a+bx} - \frac{1}{a+bLimitLow}}{-\frac{(a+bLimitHigh)(a+bLimitLow)}{2a+b(LimitHigh+LimitLow)} \left(\frac{1}{(a+bx)^2} - \frac{1}{(a+bLimitLow)^2} \right)} \right)$$

32

Where, P_a is the ambient pressure.

$$a = H - \frac{\sqrt{R_b{}^2 - y^2}}{\sin\theta}$$

$$b = -\frac{1}{\tan\theta}$$

$$LimitLow = \frac{-2R_b + \sqrt{R_b{}^2 - y^2}}{\cos\theta} - 0.05\frac{2R_b}{\cos\theta}$$

$$LimitHigh = \frac{-\sqrt{R_b{}^2 - y^2}}{\cos\theta}$$

$$W = 2 \int\limits_{y=0}^{R_b} \int\limits_{x=LimitLow}^{LimitHigh} (P - P_a)\,dxdy$$

After simplifications and cancellations shown in section 8.1, the force becomes:

$$W = 12\mu\,U\tan^2\theta \int\limits_{y=0}^{R_b} \left(-\log\left(\frac{H\sin\theta}{H\sin\theta + 2.1R_b - 2\sqrt{R_b{}^2 - y^2}} \right) - 2 + \frac{4H\sin\theta}{2H\sin\theta - 2\sqrt{R_b{}^2 - y^2} + 2.1R_b} \right) dy$$

The integration in this formula is very complex to solve analytically. Therefore, the result is obtained through numerical integration.

3.4   Finite Bearing Solution

In the finite bearing solution, the assumptions in the long bearing solution for the oil pressure zone boundaries and the gap between the bristle surface and rotor surface are used in the same manner. In long bearing solution all y-terms have been dropped. Therefore, no pressure boundary conditions are applied in y-direction, simply ignoring any effects by upstream and downstream bristles rows. However, finite bearing solution approach does not make any assumption with regard to x or y scale being dominant in the problem, and solves the full 2-D Reynolds equation (3-D bearing geometry).

Therefore, full effect of all neighboring bristles in x and y directions are considered. Similar to the long bearing solution following integration limits are applied.

$$LimitLow = \frac{-2R_b + \sqrt{R_b{}^2 - y^2}}{\cos\theta} - X_{bloom}$$

$$LimitHigh = \frac{-\sqrt{R_b{}^2 - y^2}}{\cos\theta}$$

Bristle rotor clearance is also defined the same way.

$$h = H - \frac{\sqrt{R_b{}^2 - y^2}}{\sin\theta} - \frac{1}{\tan\theta}x$$

3.4.1 Solution procedure

Consider the full 2-D Reynolds equation (3-D bearing geometry),

$$\frac{\partial}{\partial x}\left(h^3 \frac{\partial P}{\partial x}\right) + \frac{\partial}{\partial y}\left(h^3 \frac{\partial P}{\partial y}\right) = 6\mu U \frac{\partial h}{\partial x}$$

Expanding the equation above,

$$-\frac{3}{\tan\theta}h^2 \frac{\partial P}{\partial x} + h^3 \frac{\partial^2 P}{\partial x^2} + \frac{6\mu U}{\tan\theta} = \frac{-3h^2 y}{\sin\theta\sqrt{R_b{}^2 - y^2}}\frac{\partial P}{\partial y} - h^3 \frac{\partial^2 P}{\partial y^2}$$

In this equation, there are x and y variables that are independent of each other. Bearing clearance, h, is dependent on y, and linearly dependent on x. Moving the problem in to the h domain instead of x and y may simplify the solution for the

pressure. For this reason, $\frac{\partial P}{\partial x}, \frac{\partial P}{\partial y}, \frac{\partial^2 P}{\partial x^2}, \frac{\partial^2 P}{\partial y^2}$ terms are converted to $\frac{\partial P}{\partial h}, \frac{\partial^2 P}{\partial h^2}$.

$$\frac{\partial P}{\partial x} = \frac{\partial P}{\partial h}\frac{\partial h}{\partial x} = \frac{\partial P}{\partial h}\left(-\frac{1}{\tan\theta}\right)$$

$$\frac{\partial^2 P}{\partial x^2} = \frac{\partial^2 P}{\partial h^2}\left(\frac{\partial h}{\partial x}\right)^2 + \frac{\partial^2 h}{\partial x^2}\frac{\partial P}{\partial h} = \frac{\partial^2 P}{\partial h^2}\left(\frac{1}{\tan^2\theta}\right)$$

$$\frac{\partial P}{\partial y} = \frac{\partial P}{\partial h}\frac{\partial h}{\partial y} = \frac{\partial P}{\partial h}\frac{y\left(R_b{}^2 - y^2\right)^{-\frac{1}{2}}}{\sin\theta}$$

$$\frac{\partial^2 P}{\partial y^2} = \frac{\partial^2 P}{\partial h^2}\left(\frac{\partial h}{\partial y}\right)^2 + \frac{\partial^2 h}{\partial y^2}\frac{\partial P}{\partial h}$$

$$= \frac{\partial^2 P}{\partial h^2}\frac{y^2}{\left(R_b{}^2 - y^2\right)\sin^2\theta} + \frac{\partial P}{\partial h}\frac{\left(R_b{}^2 - y^2\right)^{-\frac{1}{2}} + y^2\left(R_b{}^2 - y^2\right)^{-\frac{3}{2}}}{\sin\theta}$$

When these new derivative forms are substituted, the main equation becomes:

$$-\frac{3h^2}{\tan\theta}\left(-\frac{1}{\tan\theta}\right)\frac{\partial P}{\partial h} + \frac{h^3}{\tan^2\theta}\frac{\partial^2 P}{\partial h^2} + \frac{6\mu U}{\tan\theta} = \frac{-3h^2 y}{\sin\theta\sqrt{R_b{}^2 - y^2}}\frac{\partial P}{\partial h}\frac{y\left(R_b{}^2 - y^2\right)^{-\frac{1}{2}}}{\sin\theta}$$

$$-h^3\left(\frac{\partial^2 P}{\partial h^2}\frac{y^2}{\left(R_b{}^2 - y^2\right)\sin^2\theta} + \frac{\partial P}{\partial h}\frac{\left(R_b{}^2 - y^2\right)^{-\frac{1}{2}} + y^2\left(R_b{}^2 - y^2\right)^{-\frac{3}{2}}}{\sin\theta}\right)$$

Simplify to get:

$$\frac{3h^2}{\tan^2\theta}\frac{\partial P}{\partial h} + \frac{h^3}{\tan^2\theta}\frac{\partial^2 P}{\partial h^2} + \frac{6\mu U}{\tan\theta} = \frac{\partial P}{\partial h}\frac{-3h^2 y^2}{\sin^2\theta\left(R_b{}^2 - y^2\right)} - \frac{\partial^2 P}{\partial h^2}\frac{h^3 y^2}{\left(R_b{}^2 - y^2\right)\sin^2\theta}$$

$$-\frac{\partial P}{\partial h}h^3\frac{\left(R_b{}^2 - y^2\right)^{-\frac{1}{2}} + y^2\left(R_b{}^2 - y^2\right)^{-\frac{3}{2}}}{\sin\theta}$$

Regroup and arrange the terms, it becomes:

$$\frac{\partial^2 P}{\partial h^2}\left(\frac{h^3}{\tan^2\theta} + \frac{h^3 y^2}{\left(R_b{}^2 - y^2\right)\sin^2\theta}\right) = -\frac{6\mu U}{\tan\theta} + \frac{\partial P}{\partial h}\left(\begin{array}{c} \dfrac{-3h^2 y^2}{\sin^2\theta\left(R_b{}^2 - y^2\right)} - \dfrac{h^3}{\left(R_b{}^2 - y^2\right)^{\frac{1}{2}}\sin\theta} \\[4mm] -\dfrac{h^3 y^2}{\left(R_b{}^2 - y^2\right)^{\frac{3}{2}}\sin\theta} - \dfrac{3h^2}{\tan^2\theta} \end{array}\right)$$

As a result, the equation is in the form of:

$$\frac{\partial^2 P}{\partial h^2}A = \frac{\partial P}{\partial h}B + C \Rightarrow \frac{\partial^2 P}{\partial h^2} = \frac{\partial P}{\partial h}\frac{B}{A} + \frac{C}{A} \Rightarrow \frac{\partial^2 P}{\partial h^2} = \frac{\partial P}{\partial h}D + E$$

A and B are functions of h(x,y), y, R_b and θ. C is constant since θ, μ and U do not change in the equation. For further simplification, it is considered that $y = kR_b$ (That is, y varies in increments of R_b), A and B becomes:

$$A = \frac{h^3}{\tan^2\theta} + \frac{h^3 k^2 R_b^{\,2}}{\left(1-k^2\right)R_b^{\,2}\sin^2\theta} = \frac{h^3}{\tan^2\theta} + \frac{h^3 k^2}{\left(1-k^2\right)\sin^2\theta} = \frac{h^3\cos^2\theta\left(1-k^2\right)+h^3 k^2}{\left(1-k^2\right)\sin^2\theta}$$

$$= \frac{h^3\cos^2\theta + h^3 k^2\sin^2\theta}{\left(1-k^2\right)\sin^2\theta}$$

$$B = \frac{-3h^2 k^2 R_b^{\,2}}{\left(1-k^2\right)R_b^{\,2}\sin^2\theta} - \frac{h^3}{\left(1-k^2\right)^{\frac{1}{2}}R_b\sin\theta} - \frac{h^3 k^2 R_b^{\,2}}{R_b^{\,3}\left(1-k^2\right)^{\frac{3}{2}}\sin\theta} - \frac{3h^2}{\tan^2\theta}$$

$$= \frac{-3h^2 k^2}{\left(1-k^2\right)\sin^2\theta} - \frac{h^3}{\left(1-k^2\right)^{\frac{1}{2}}R_b\sin\theta} - \frac{h^3 k^2}{R_b\left(1-k^2\right)^{\frac{3}{2}}\sin\theta} - \frac{3h^2}{\tan^2\theta}$$

$$B = \frac{h^2}{\left(1-k^2\right)^{\frac{3}{2}}R_b\sin^2\theta}\left(-3k^2 R_b\left(1-k^2\right)^{\frac{1}{2}} - h\left(1-k^2\right)\sin\theta - hk^2\sin\theta - 3\left(1-k^2\right)^{\frac{3}{2}}R_b\cos^2\theta\right)$$

$$B = \frac{h^2}{\left(1-k^2\right)^{\frac{3}{2}}R_b\sin^2\theta}\left(-3k^2 R_b\left(1-k^2\right)^{\frac{1}{2}} - h\sin\theta - 3\left(1-k^2\right)^{\frac{3}{2}}R_b\cos^2\theta\right)$$

$$= \frac{-h^2\left(h\sin\theta + 3R_b\left(1-k^2\right)^{\frac{1}{2}}\left(k^2 + \left(1-k^2\right)\cos^2\theta\right)\right)}{\left(1-k^2\right)^{\frac{3}{2}}R_b\sin^2\theta}$$

$$D = \frac{B}{A} = \frac{-h^2\left(h\sin\theta + 3R_b\left(1-k^2\right)^{\frac{1}{2}}\left(k^2\sin^2\theta + \cos^2\theta\right)\right)}{\left(1-k^2\right)^{\frac{3}{2}}R_b\sin^2\theta} \cdot \frac{\left(1-k^2\right)\sin^2\theta}{h^3\left(\cos^2\theta + k^2\sin^2\theta\right)}$$

$$= \frac{-\left(\frac{h\sin\theta}{\left(\cos^2\theta + k^2\sin^2\theta\right)} + 3R_b\left(1-k^2\right)^{\frac{1}{2}}\right)}{\left(1-k^2\right)^{\frac{1}{2}}R_b h} = \frac{-\sin\theta}{R_b\left(\cos^2\theta + k^2\sin^2\theta\right)\sqrt{1-k^2}} - \frac{3}{h}$$

$$E = \frac{C}{A} = -\frac{6\mu U}{\tan\theta}\frac{\left(1-k^2\right)\sin^2\theta}{h^3\left(\cos^2\theta + k^2\sin^2\theta\right)} = \frac{-3\mu U\left(1-k^2\right)\sin 2\theta}{h^3\left(\cos^2\theta + k^2\sin^2\theta\right)}$$

Since both D and E are functions of h(x,y) and y, this equation requires numerical solution to obtain the pressure and the lift force results. Adapting the equations for numerical scheme:

$$\frac{\frac{\partial P}{\partial h} - \left(\frac{\partial P}{\partial h}\right)^{-}}{\Delta h} \cong \frac{\partial^2 P}{\partial h^2} = \frac{\partial P}{\partial h} D + E \;.$$

Upper score means value from previous iteration. Similarly, double upper score means parameter value from two iterations earlier should be considered. Since the pressure calculation code first gives the number for y and then x, at a calculation cycle x is changed in time. Since h is linearly dependent on x, changing the x at a constant rate changes h also at a constant rate. This means dh changes with a constant slope with respect to x, so dh in $\frac{\partial P}{\partial h}$ and $\left(\frac{\partial P}{\partial h}\right)^{-}$ are the same.

$$\frac{P - P^{-} - (P^{-} - P^{--})}{(\Delta h)^2} - \frac{P - P^{-}}{\Delta h} D = E$$

$$\frac{P}{(\Delta h)^2} - \frac{P}{\Delta h} D = E + P^{-}\left(\frac{2}{(\Delta h)^2} - \frac{D}{\Delta h}\right) - \frac{P^{--}}{(\Delta h)^2}$$

$$P = \frac{E + P^{-}\left(\dfrac{2}{(\Delta h)^2} - \dfrac{D}{\Delta h}\right) - \dfrac{P^{--}}{(\Delta h)^2}}{\dfrac{1}{(\Delta h)^2} - \dfrac{D}{\Delta h}}$$

Finally,

$$P = \frac{E(\Delta h)^2 + P^{-}(2 - D\Delta h) - P^{--}}{1 - D\Delta h}$$

Now we can numerically integrate pressure to obtain lift force,

$$W = 2 \int_{y=0}^{Integration\,Limit\,for\,y} \int_{x=LimitLow}^{LimitHigh} P\,dx\,dy$$

Integration limit in y direction in the integral above is determined with the axial distance (along the rotor) from the center line of the bristle row in consideration to the surface of the neighboring bristle. This axial spacing varies with the amount of axial bloom as will be discussed in the following sections.

4   VALIDATION

Direct measurement of lift force or lift clearance in brush seals is not possible. However, there are experimental data available for leakage as a function of shaft speed.
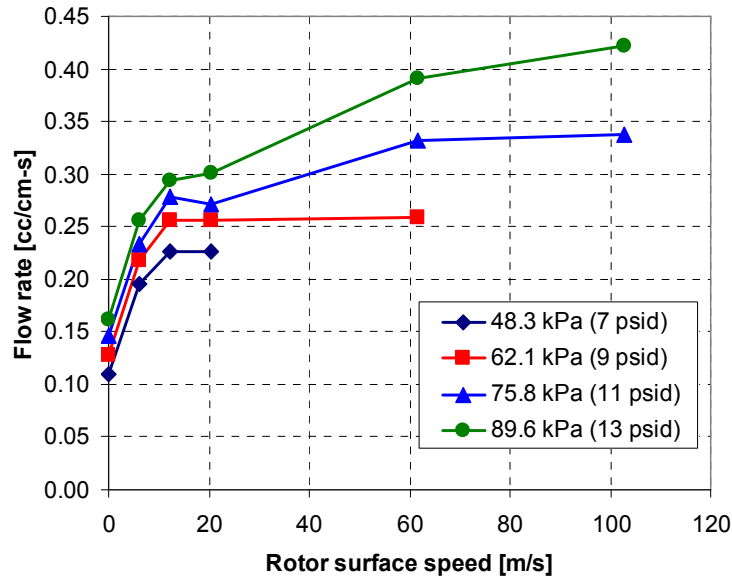

Figure 16: Flow rate measurement of an oil brush seal vs. rotor surface speed [40].

As illustrated in the Figure 16, data presented by Aksit et al. [40] indicates that the leakage increases rapidly with rotor speed, and levels of at higher speeds due to shear thinning of oil. Under certain conditions, although slow, leakage may continue to rise at higher speeds. This may be due to the blooming of the bristles which is out of scope of this work.

Studying the experimental leakage data, one might conclude that static line to line leakage is the oil flow rate through the bristle pack. Additional leakage observed upon introduction of the rotor speed can be attributed to the leakage through the hydrodynamic lift clearance between the rotor and the seal. Using this leakage data it is possible to calculate lift clearance observed during these tests. Hydrodynamic lift clearance data obtained form these test results can be utilized to compare and validate analysis results presented here.

Using the clearance values obtained from experimental leakage data two different approaches can be used to validate analyses presented here. One approach is to use the observed lift clearance for the tested seal, and calculate corresponding lift force. Then

this lift force can be compared with other analyses results or simple beam solutions. The other approach is to use the bristle tip force calculated from beam theory or based on other analyses, then estimate and compare the lift clearance. It should be noted that bristle forces due to bristle bending, blow down, inclined prop and other effects will become balanced/equal to the hydrodynamic lift forces when the bristle tip reaches the steady clearance from the rotor surface. Because of the unknowns involved in bristle tip force in the presence of oil, the first approach will be used here for validation purposes.

4.1 Calculation of Lift Clearance from Leakage Measurements

As reported before, in the absence of any measured hydrodynamic oil lift force the approach to validate analyses results will be to use the observed lift clearance for the tested seal, then calculate and compare the corresponding lift force. It is possible to obtain hydrodynamic lift clearance from the measured oil leakage rates for the brush seals. Leakage rate can be converted to the clearance value through the Poiseuille flow formulation for a fluid flow under the known pressure difference across the gap.
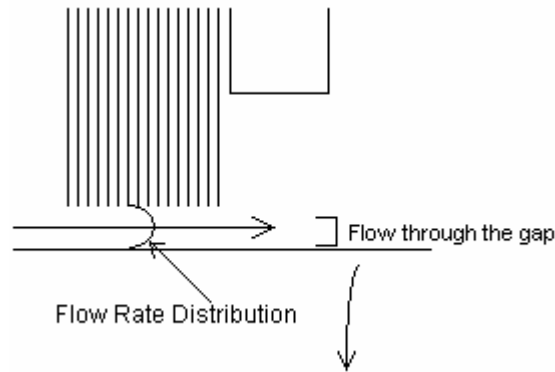

Figure 17: Representative flow through the bristle tip clearance.

Duran et al. [11] has formulated the velocity profile at the bristle tip clearance from Navier-Stokes equations as follows:

$$V_y = \frac{1}{2\mu} \frac{\partial P}{\partial y} \left(z^2 - zH \right).$$

Total leakage flow through tip clearance can be obtained by integrating the velocity profile across the gap:

$$Q_{perlength} = \left| \int_{z=0}^{H} V_y dz \right| = \frac{H^3}{12\mu} \frac{\Delta P}{t_{brushseal}} \left(z^2 - zH \right).$$

Viscosity in this equation is a strong function of oil. However there is a lack of experimental data for temperature with respect to speed and pressure. As expressed earlier, calculation of viscous heat dissipation and variation of temperature through the gap is out of scope of this work. Therefore, measured temperature rise data will be used to calculate effective oil viscosity. According to the work by Aksit et al. [40] viscosity of the oil used in the experiments is determined for 50 °C oil temperature as:

$$\mu = 0.028 e^{-0.0294*(50-37.78)} = 0.0195 Pa-s \,.$$

For a brush seal with thickness $t_{brushseal}$=1.484mm, the flow rate data supplied by Aksit et al. [40] is as in Table 1.

Raw Flow Rate (cm^3/s/cm)		Pressure			
		48.3kPa (7psid)	62.1kPa (9psid)	75.8kPa (11psid)	89.6kPa (13psid)
Velocity	0m/s	0,109	0,128	0,147	0,162
	6.2m/s	0,196	0,218	0,233	0,256
	12.5m/s	0,226	0,256	0,278	0,293

Table 1: Flow rate vs. pressure and velocity.

Since there is no hydrodynamic lift of the bristles for the static case, leakage value listed zero velocity is the flow through the bristles as shown in Figure 17. This through bristle leakage is considered to be constant under constant pressure, regardless of the rotor surface speed.
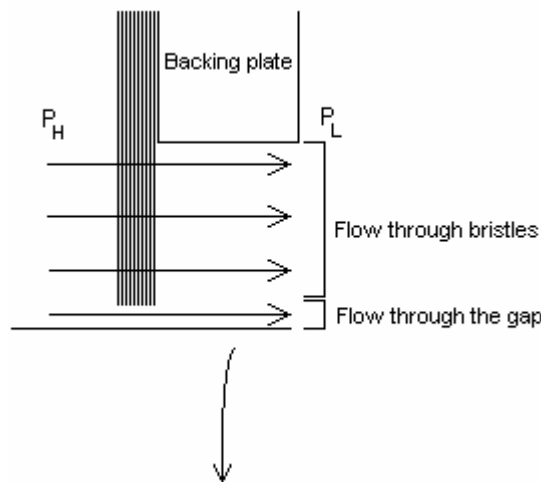

Figure 18: Leakage flow in the brush seal.

For a brush seal with thickness of $t_{brushseal}$=1.484mm, with due consideration for the flow through the bristles, the flow rate data supplied by Aksit et al. [40] are converted to the bristle tip clearance information using the flow relations given above.

Clearance (mm)		Pressure			
		48.3kPa (7psid)	62.1kPa (9psid)	75.8kPa (11psid)	89.6kPa (13psid)
Velocity	0m/s	0	0	0	0
	6.2m/s	0,04	0,037	0,034	0,033
	12.5m/s	0,044	0,042	0,039	0,037
	20.5m/s	0,044	0,042	0,038	0,038

Table 2: Clearance vs. pressure and velocity.

Hydrodynamic lift clearance values are tabulated in Table 2 and plotted in Figure 19. The results are also compared with those of a CFD solution provided in reference [40]. Data indicate that the lift stabilizes at around 40-50 microns.
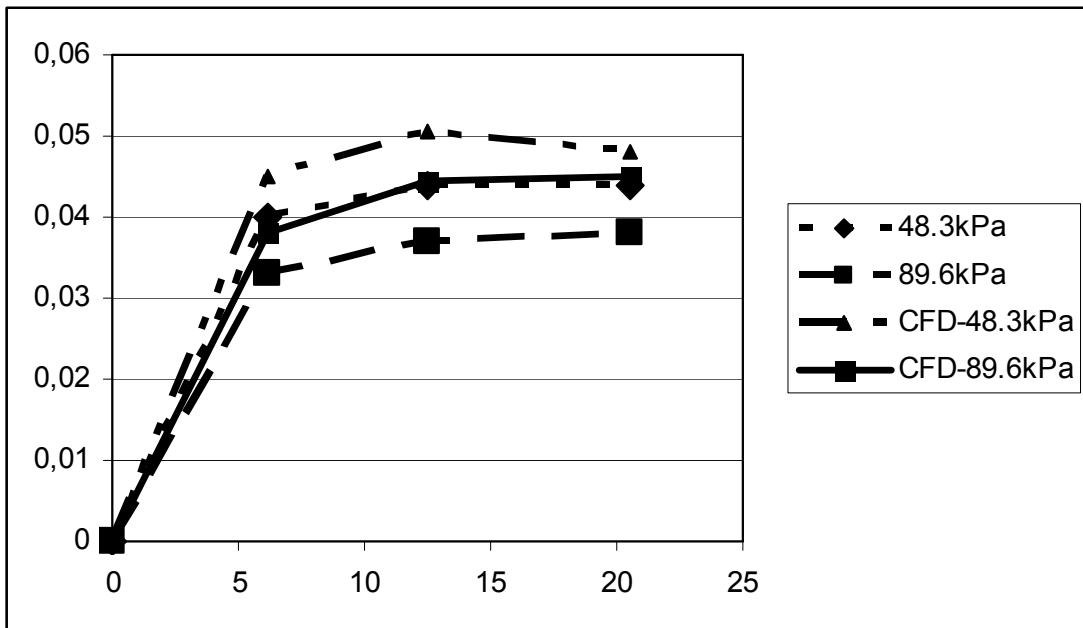

Figure 19: Clearance vs. Rotor Surface Speed.

4.2 Bristle Bending Force Calculation through Beam Theory

Once the lift clearance is known hydrodynamic lift force can be calculated using short, long or finite bearing analyses presented earlier. However, these forces should be compared with the balancing beam bending and other reaction forces that would keep bristle in equilibrium during operation. The simplest way to do this is to compare their magnitude with the beam bending reaction. The bending force on a bristle can be formulated using simple beam theory [40]. As the bristle tip lifting is even smaller than %1 of the bristle length simple beam theory would be valid. The main formula of the beam theory is as follows [41]:

$y_d = \dfrac{F_b L^3}{3EI}$ where F_b is the normal force acting to the bristle tip, L is the length of the

bristle and E is the modulus of elasticity of the bristle material. I is the inertia $I = \dfrac{\pi d^4}{64}$

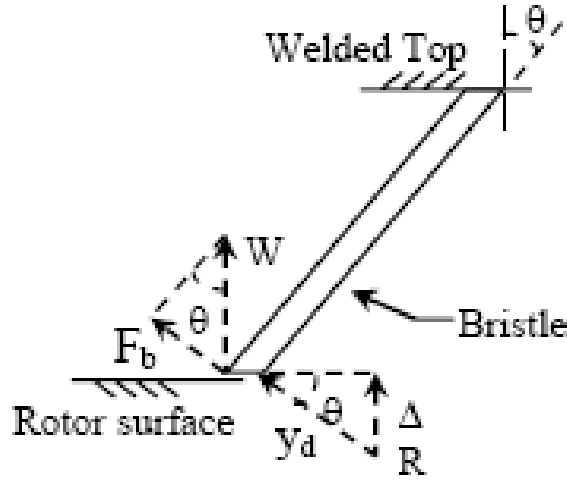where d is the diameter of the bristle.

Figure 20: Forces and motions in the beam theory [40].

Observing from Figure 20 [40] that $y_d = \dfrac{\Delta R}{\sin \theta}$ and $W = \dfrac{F_b}{\sin \theta}$ beam deflection force

can be obtained by [41]:

$W = \dfrac{F_b}{\sin \theta} = \dfrac{3EIy_d}{L^3} \dfrac{1}{\sin \theta} = \dfrac{3E}{L^3} \dfrac{\pi d^4}{64} \dfrac{\Delta R}{\sin \theta} \dfrac{1}{\sin \theta} = \dfrac{3\pi}{64} \dfrac{Ed^4 \Delta R}{L^3 \sin^2 \theta}$ where ΔR is the

clearance of the bristle tip from the rotor surface (h).

4.3   Calculation of the Blow-down Force on the Bristles

Beam theory, alone, would underestimate the bristle tip reaction as it does not account for other forces like blow-down, bristle interlocking and friction. The force induced by the radial flow from the bristle root towards the bristle tips as in Figure 21 is called blow-down [15]. This effect has been studied by Wood [42], Chen et al. [37], Bayley and Long [35], and Turner et al. [43]. Due to the cant angle, the bristles do also have horizontal component of the area. The pressure within the brush pack varies with both the radial and axial position, so there is always a difference between the pressures at the upper and lower sides of the bristle. This pressure difference produces some downward force on each section of the bristle, and these forces create a downward moment on the bristles. This moment helps pressing the bristle tip down to the rotor surface. The effect of the blow-down force on the bristle tip can be calculated by dividing the vertical moment on the bristle by the horizontal component of the length of the bristle.
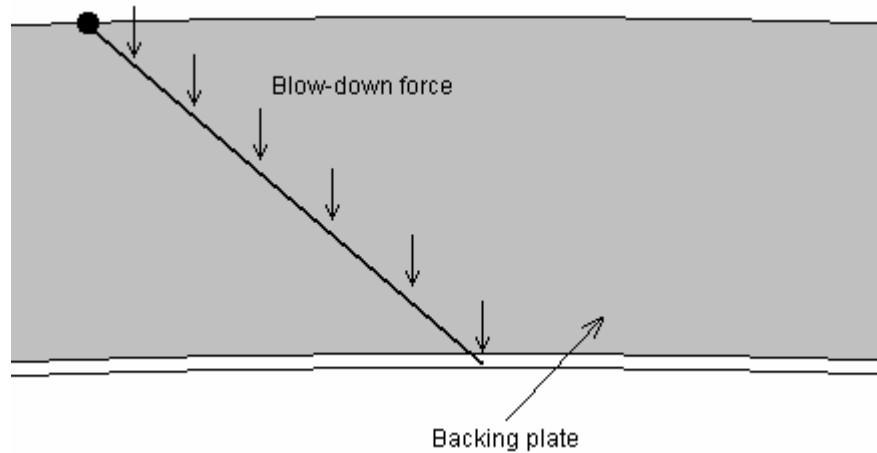

Figure 21: Blow-down force.

In order to calculate the blow-down force on the bristle tips, it is necessary to know pressure in every section of the brush seal. Experimental data by Braun et al. [44, 45] and Bayley and Long [35] propose that the axial pressure drop between the high pressure and back plate pressure zones and between the high pressure and low pressure zones are almost linear as illustrated in Figure 22.
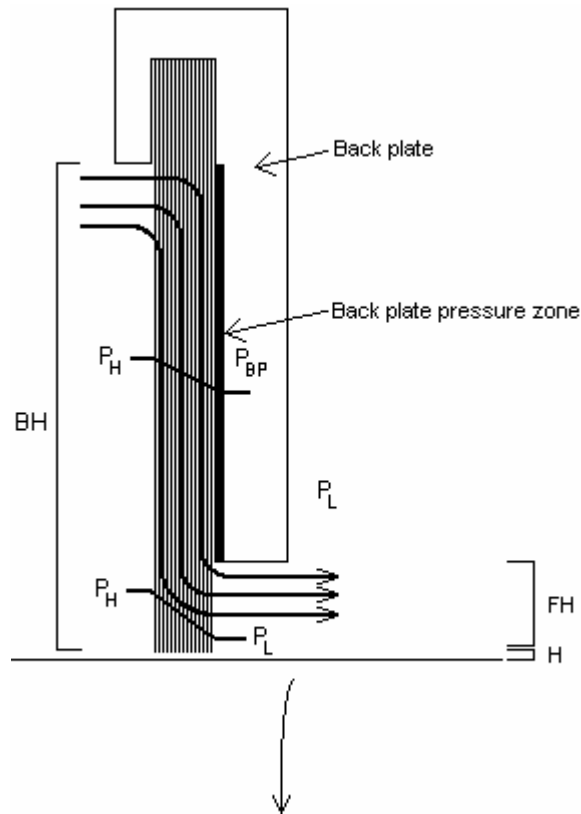
Figure 22: Schematic of brush seal axial pressure distribution.

The pressure needs to be calculated according to the high pressure - low pressure linearity below the fence height (FH), and according to the high pressure - back plate pressure linearity between the fence height and bristle height (BH). In order to obtain the pressure distribution on the back plate pressure zone, Bayley et al. [35] and Turner et al. [46] have put pressure taps on the backing plate. They have found that at the back plate pressure zone, the pressure is very near to the high pressure value immediately above the fence height. Bayley et al. [35] reported nondimensional data of the pressure distribution at the back plate pressure zone in terms of the high pressure value. This data has been measured for air. However, somewhat similar profile is expected for oil as well. Back plate pressure data provided by Bayley et al. [35] is plotted in Figure 23. The horizontal axis, r_y, is the ratio of the radial distance from the fence height to the distance between the fence height and bristle height. The vertical axis, $R_{\mathrm{Pr}essure}$, shows the ratio of the pressure at the backing plate surface to the high pressure upstream.
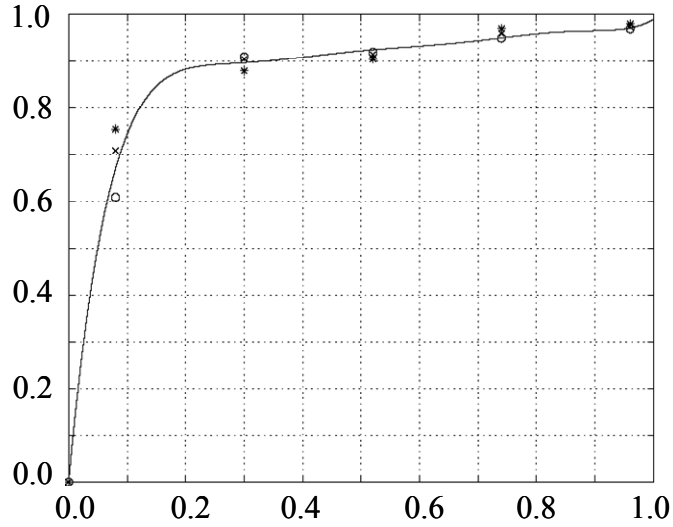
44

Figure 23: Back plate pressure zone normalized pressure distribution.

Aksit [7] has formulized the information in the graph (Figure 23) as:

$$R_{\text{Pr}essure} = 92.9847r_y{}^7 - 378.6135r_y{}^6 + 637.1967r_y{}^5 - 572.4562r_y{}^4 + 295.333r_y{}^3$$
$$- 87.1507r_y{}^2 + 13.6926r_y + 0.0034$$

As illustrated in Figure 24, with the knowledge of the pressure at a point and the height of the points from the rotor surface, it is possible to find the pressure difference at a point on the bristle as well as the total radial inward moment on the bristle due to the blow-down. The force at the bristle tip due to the blow-down is the quotient of this moment to the horizontal component of the bristle length.
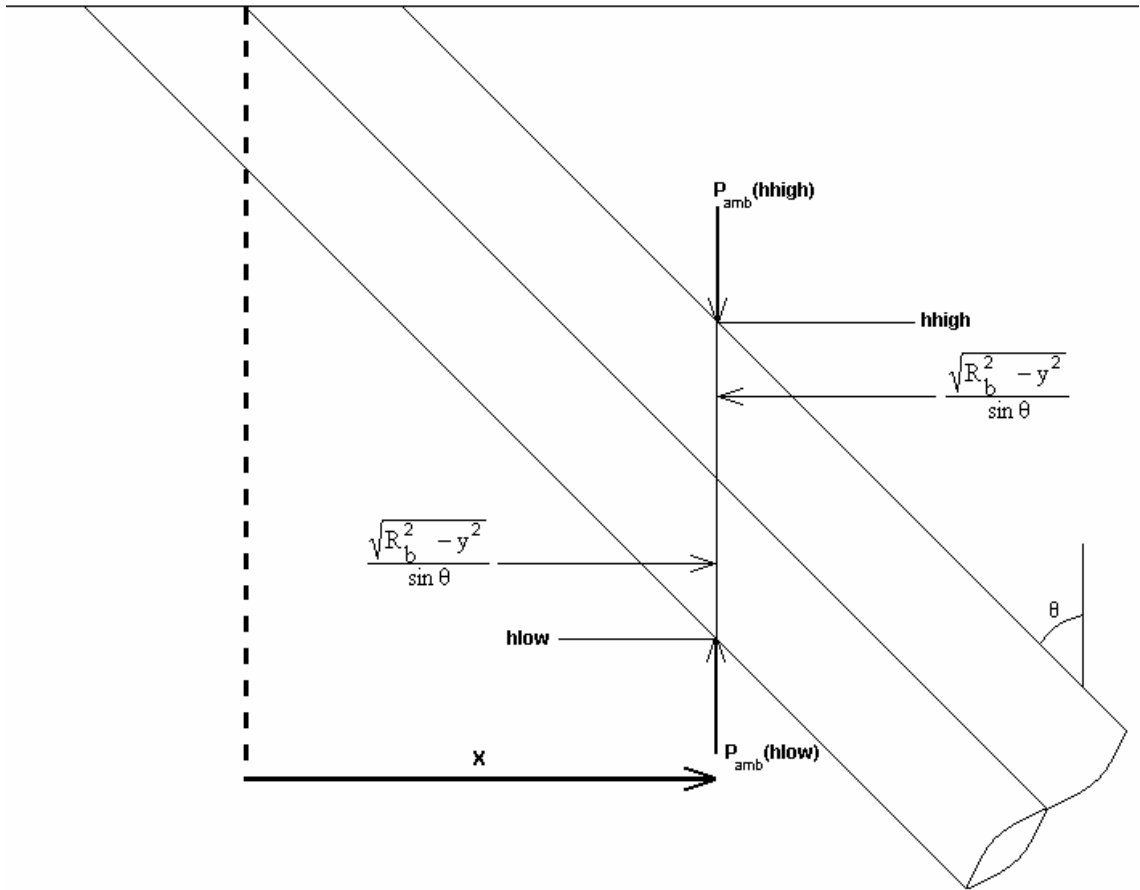
45

Figure 24: Blow-down Force Calculation.

To find the height of a point within the brush pack, the following geometric relations can be used.

$$hhigh(x, y) = H + \frac{\sqrt{R_b^2 - y^2}}{\sin \theta} - \frac{1}{\tan \theta} x$$

$$hlow(x, y) = H - \frac{\sqrt{R_b^2 - y^2}}{\sin \theta} - \frac{1}{\tan \theta} x$$

In Figure 24, it is seen that the differential slices for the calculation of the moment are vertical instead of being normal to the bristle's axis. Since the bristle bending is so small, the bristle behaves similar to a straight cantilever beam. In such a case the vertical component of the effect of either kind of slice integration would be nearly same. Since the integration of vertical slices is both less complicated and gives reasonable result, it is used to solve the force on the bristle tip due to the blow-down effect.

46

4.4 Effect of Staggered Bristles

There are two possibilities to model the arrangement of the bristles in a brush seal: In-line configuration and staggered configuration. They are depicted in Figure 25:
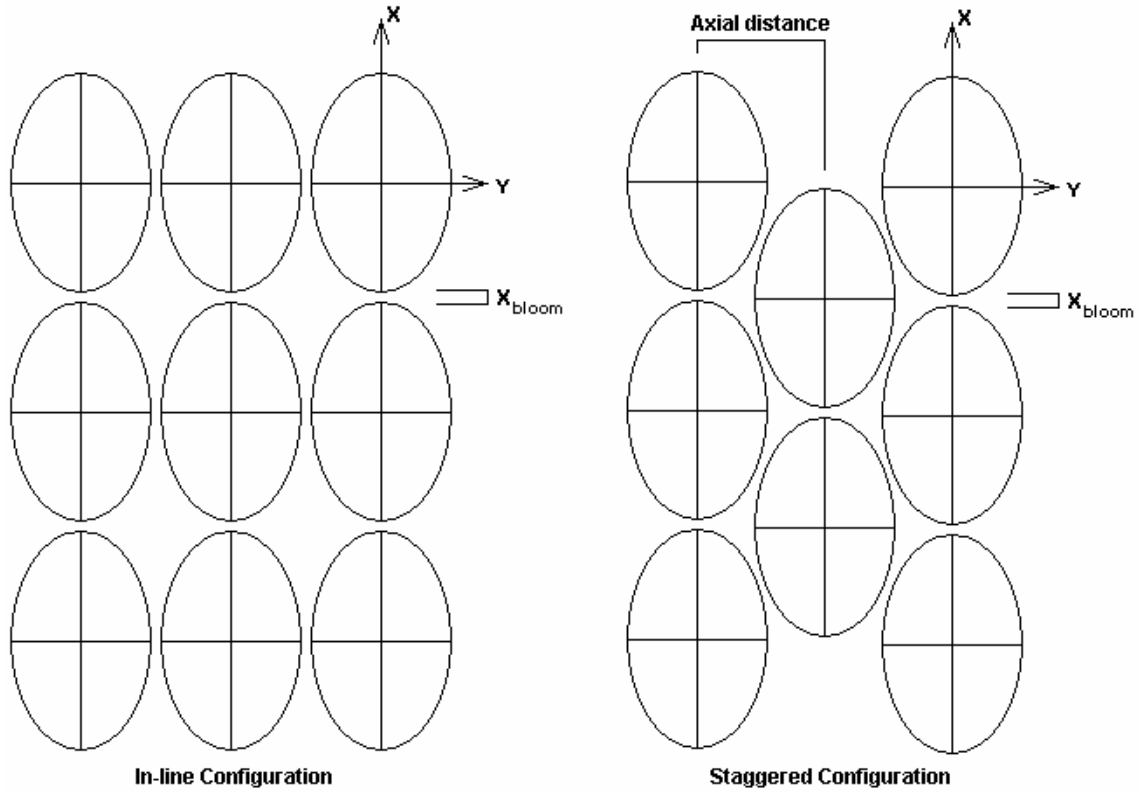

Figure 25: Footprints of the bristle arrangement models in the brush seal.

In reality, when bristles are packed tightly, and stowed between the retaining and backing plates, they naturally form the staggered configuration due to their round sections. This configuration is the reason for the dominant effects of the inter-bristle locking. In this configuration, the bristles do have large surfaces to rub on each other. This results in interlocking which limits their motion in radial direction during a rotor excursion. However, formulations in the staggered configuration are more complex due to the complexity of the leakage through the bristles which also involves motion in axial (y) direction.

In a typical layout, there are two bristle spacing values that need to be considered. Both of these values are important as they also affect integration limits during analytical solutions. The distance between subsequent bristles in the same circumferential row is called the X_{bloom} as shown in Figure 25 above. It is the distance between the bristles in the x direction. Aksit [7] reported that the X_{bloom} is around 5% of the minimum distance

47

between the centers of the bristles, which means 0.05d looking down normal to the bristle axes as in Figure 26 below. This distance is determined by the manufacturing process and remains similar for most seals. On the other hand, axial spacing between the interlocked adjacent bristle rows varies with operating conditions and seal design. This distance is called the axial bloom (Y_{bloom}). When bristles are fully packed under the pressure loads, this minimum axial distance is $1.717R_b$ (see Figure 26).
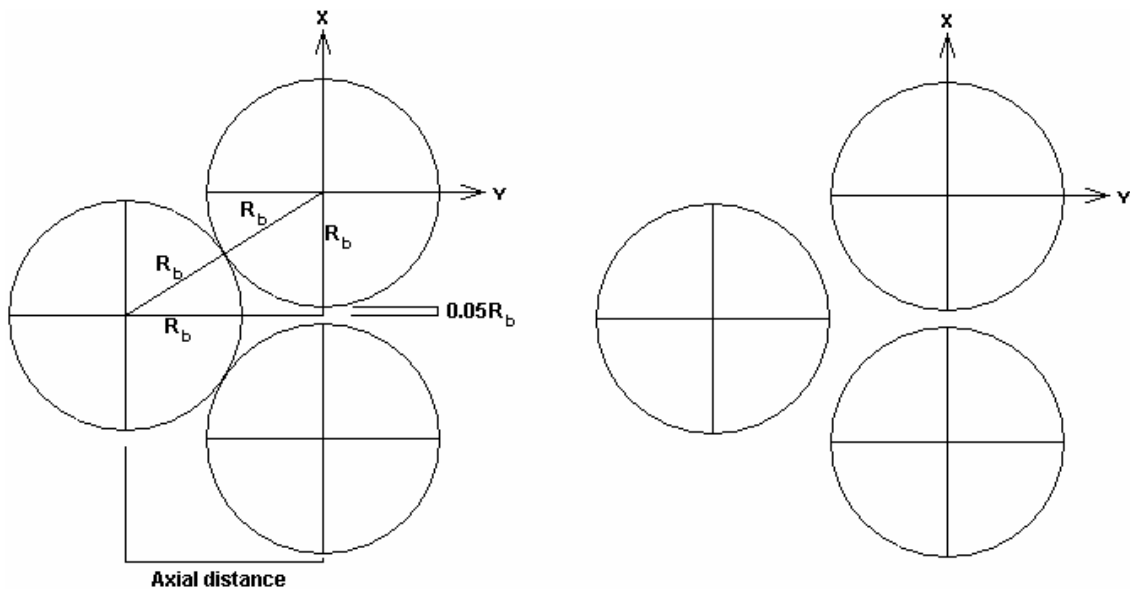

Figure 26: Effect of the axial bloom.

In the finite bearing solution, amount of axial bloom is critical, as it determines the integral limits in y direction. Actual value of the axial bloom is very difficult to solve since it changes with bristle geometry and load conditions. Effect of axial bloom on finite bearing solution will be discussed in the following section.

5   RESULTS AND DISCUSSION

As indicated earlier, analyses results are verified based on the available dynamic oil leakage data. To make a valid comparison, the following design parameters (which represent the available test seal) have been used in evaluating analytical solutions.

Bristle material	Haynes 25
Bristle elasticity	206.8 GPa
Average number of bristles in axial direction	16
Cant angle	45º
Bristle diameter	0.102mm
Fence height	0.762mm
Bristle height	10.668mm
Input oil temperature	50ºC
Oil viscosity at 50ºC	0.0195Pa-s

Table 3: Test parameters used in analyses.

The type of the oil is Mobil DTE-24 as indicated in reference [40] where test data have been presented. Oil properties were taken from the manufacturer web site [47]. Using the parameters tabulated in Table 3, pressure distribution for each analysis approach can be obtained. For a 38μm bristle tip clearance and 20.5m/s rotor surface speed, oil pressure distribution obtained for short bearing, long bearing and finite bearing formulations are presented in Figures 27, 28 and 29 respectively.
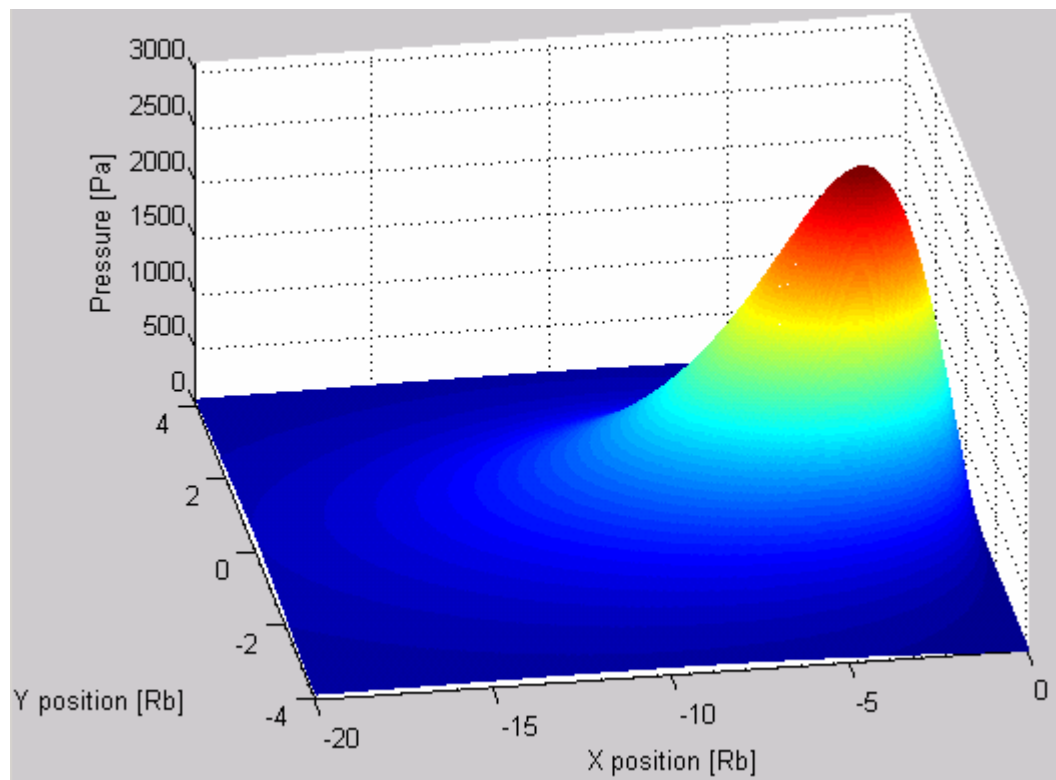

Figure 27: Oil lift pressure distribution under the bristles using short bearing approach.
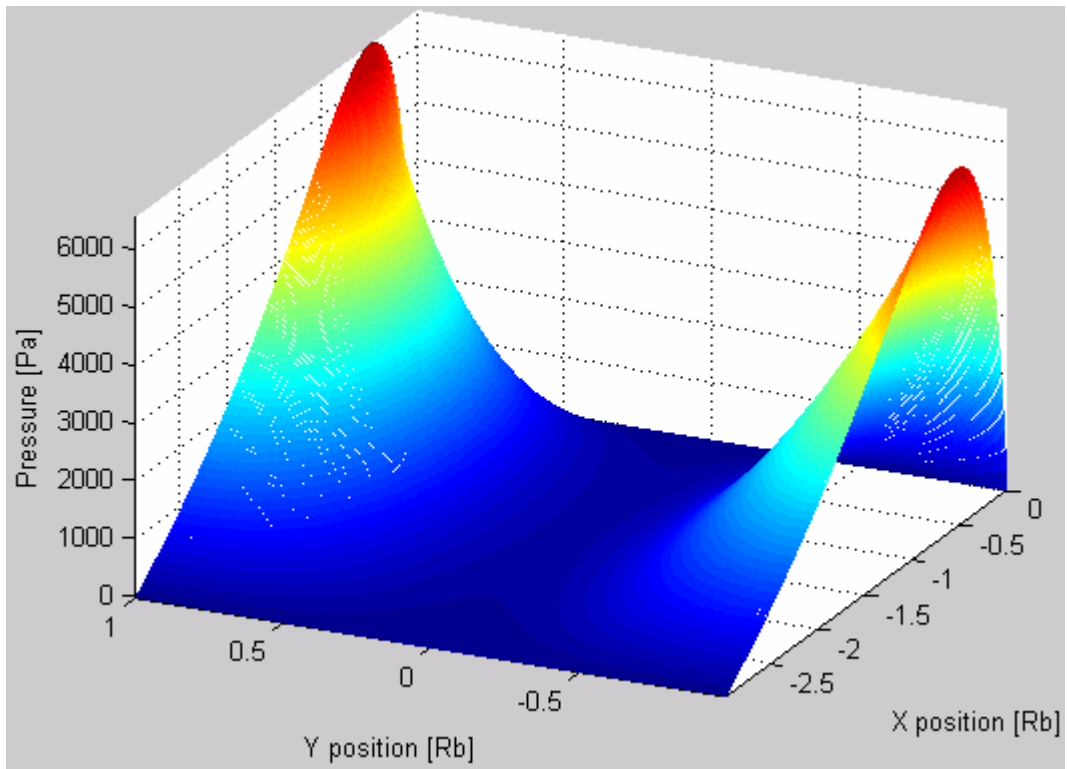
Figure 28: Oil lift pressure distribution under the bristles using long bearing approach.
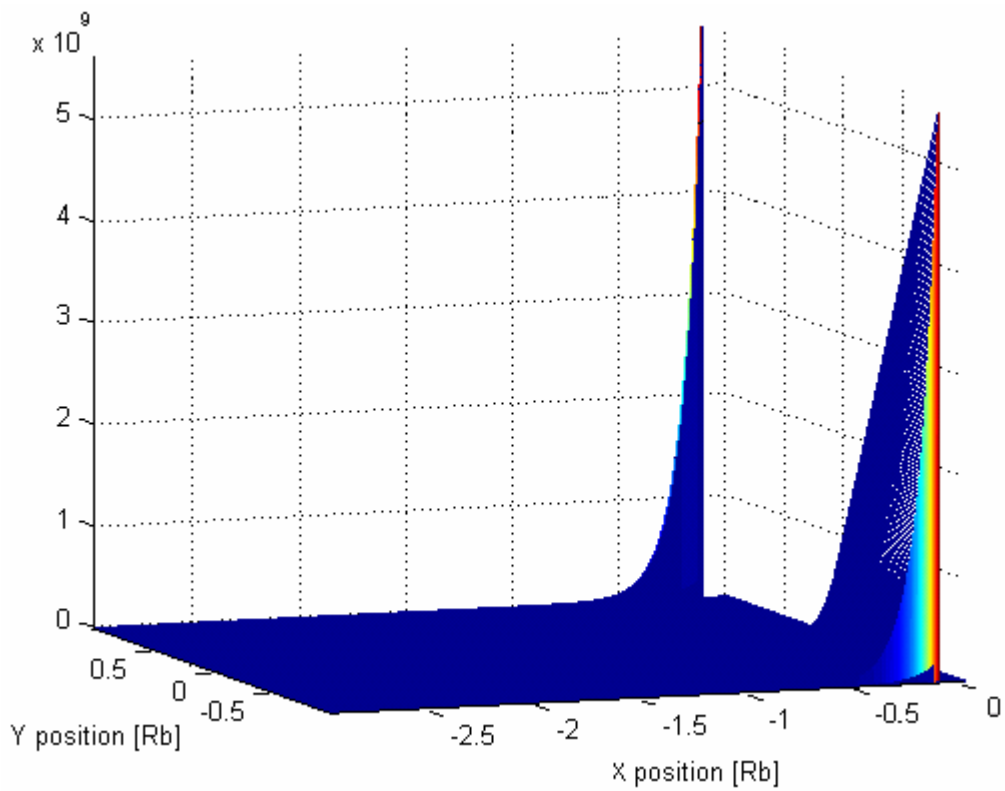

Figure 29: Oil lift pressure distribution under the bristles using finite bearing approach.

As observed from the figures, pressure distribution obtained using the short bearing approach peaks along the centerline under the bristle. This is typical of most bearings. Short bearing approach considers only a single bristle where oil pumped by the rotating shaft is squeezed near the bristle tip. Since adjacent rows are ignored, pressure decreases very fast when approached to the sides of the bristle. Boundary conditions require oil pressure to drop down to ambient at either side of the bristle.

On the other hand, the pressure distributions obtained for long bearing and finite bearing approaches peak at either end of the bristle. In both long bearing and finite bearing formulations the inter bristle gap between the consecutive bristles in a same circumferential row gets very small (around 5% of the bristle diameter). The very small gap in the middle of the bearing section at the bristle tip limits the penetration of the oil pumped by the rotor yielding a smaller hydrodynamic pressure at the mid section. As moved towards either side of the bristle centerline, circumferential distance between the bristles increase rapidly allowing higher hydrodynamic oil pressures to develop. As a result, pressure profiles peak at either side of the bristle as presented in Figures 28 and 29.

In the pressure distribution graph of the long bearing solution, it is observed that the pressure develops in a fairly homogenous manner when compared to the pressure distribution graph of the finite bearing solution. The long bearing solution is based on the assumption that bearing surface is very long in axial (y) direction, thereby ignoring any axial oil flows from the middle of the bristles to the sides. In fact, long bearing approach is an attempt to obtain a closed form simplified solution to the Reynolds Equation by eliminating y-dependent terms taking advantage of aspect ratios indicating bearing length in x-direction (circumferential gap between consecutive bristles in the same row) gets very small compared to the bearing length in y-direction (that is the bristle diameter) when bristles are tightly packed, and only the very small tip portion is exposed to act as a bearing.

On the other hand, the finite bearing assumption takes all of the flow components into consideration, so there is a large amount of oil flow from the center to the outer sections. Oil flow is further squeezed at either ends when blocked by the neighboring bristles, leading to sharp increases in oil pressure at either side. As a result finite bearing approach yields much larger hydrodynamic oil lift pressure results compared to the long bearing solution. It should also be noted that as moved from center to either side of the bristle, x-spacing between the subsequent bristles get larger and larger. Therefore, width

of the bearing (d) is not very long compared to the wedge distance (x) at outer ends. In other words, long bearing assumption loses its validity as moved away from the centerline.

In order to illustrate behavior of each analytical solution at increased speeds, analyses were repeated for various rotor speeds. As presented in Chapter 3 on solution procedures, analytical solutions are obtained for constant effective temperature. Therefore, if shear heating with increasing rotor speed is ignored, oil temperature and oil viscosity will remain constant leading to a solution that estimates lift forces indefinitely increasing with rotor speeds. For constant viscosity, change in calculated hydrodynamic lift forces with rotor speeds based on short bearing, long bearing and finite bearing solutions are presented in Figures 30, 31, 32, 33, 34 and 35 respectively.
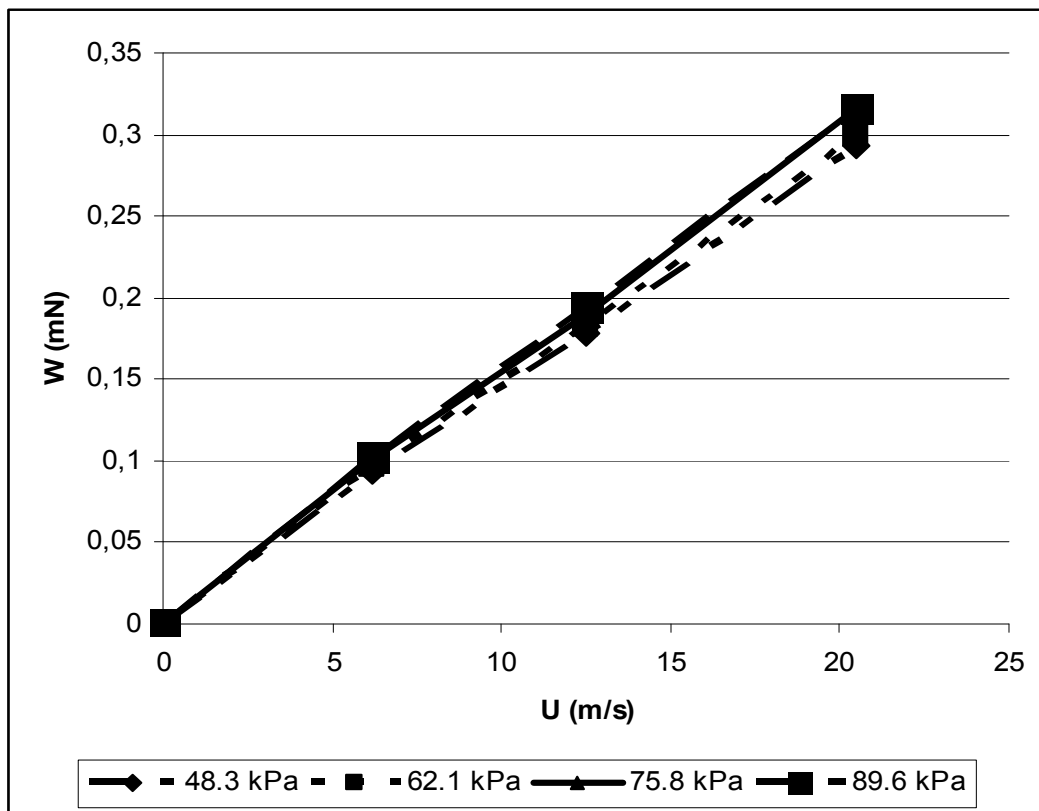

Figure 30: Hydrodynamic lift vs. speed for constant viscosity short bearing assumption.
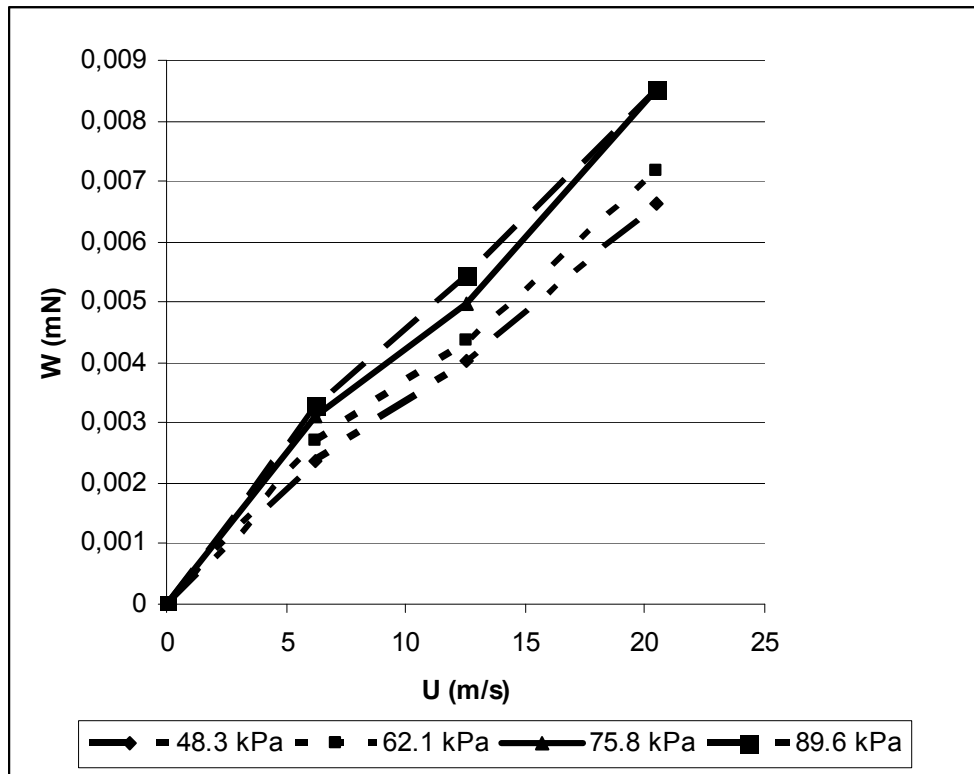
Figure 31: Hydrodynamic lift vs. speed for constant viscosity long bearing assumption.

Because of the fact that finite bearing approach incorporates all the terms in Reynolds Equation, integration limits in y (axial) direction change with the distance between the adjacent bristle rows, i.e. the axial bloom. As mentioned before, circumferential distance between the consecutive bristles in the same circumferential row increase rapidly allowing higher hydrodynamic oil pressures to develop at either ends. Therefore, calculated hydrodynamic lift force increases with increasing axial bloom rates. From Figures 32 to 34 various lift force estimates are presented based on different axial bloom rates. Knowledge of actual axial bloom rates under specific loading conditions require a separate detailed mechanical bristle deflection analysis which is beyond the scope of this work.
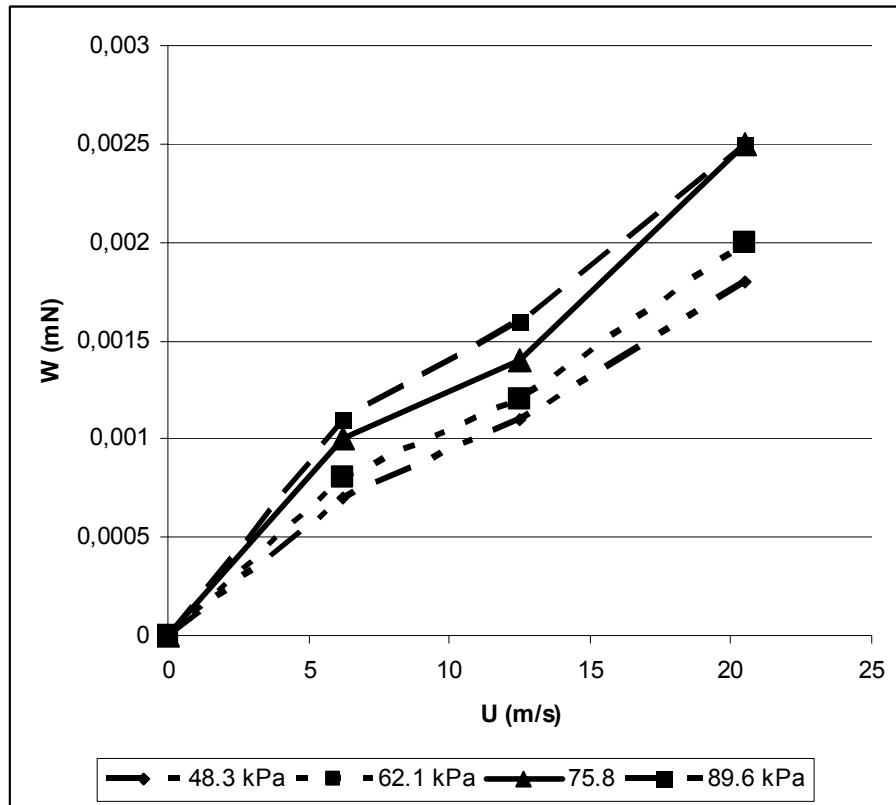
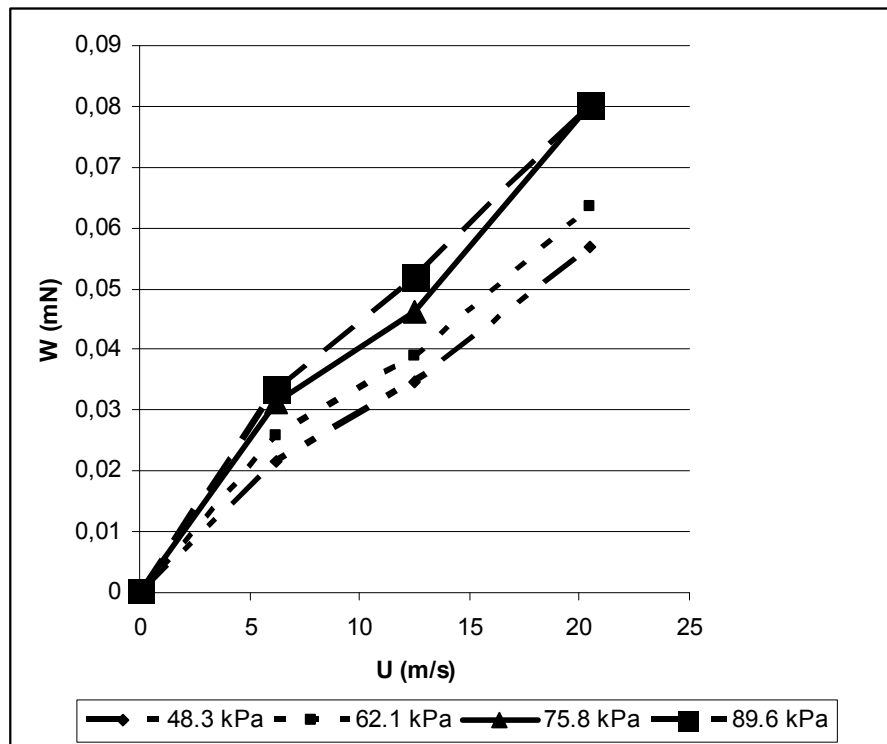Figure 32: Hydrodynamic lift vs. speed for constant viscosity finite bearing assumption no axial bloom.

Figure 33: Hydrodynamic lift vs. speed for constant viscosity finite bearing assumption 15% axial bloom.
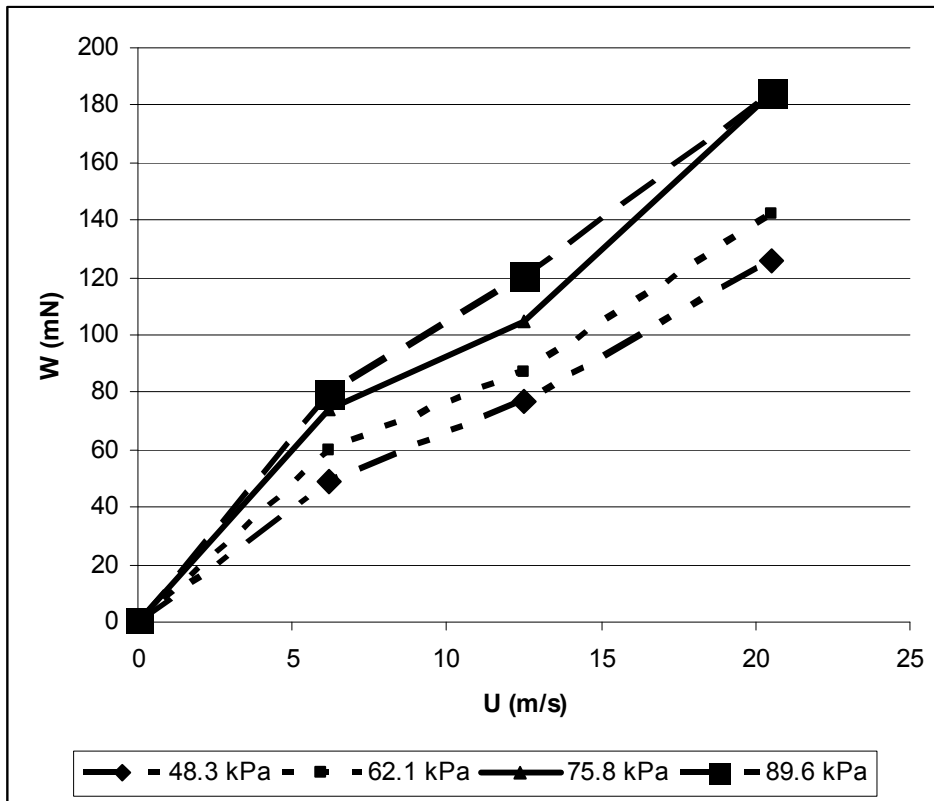
Figure 34: Hydrodynamic lift vs. speed for const. viscosity finite bearing assumption 15.8% axial bloom.
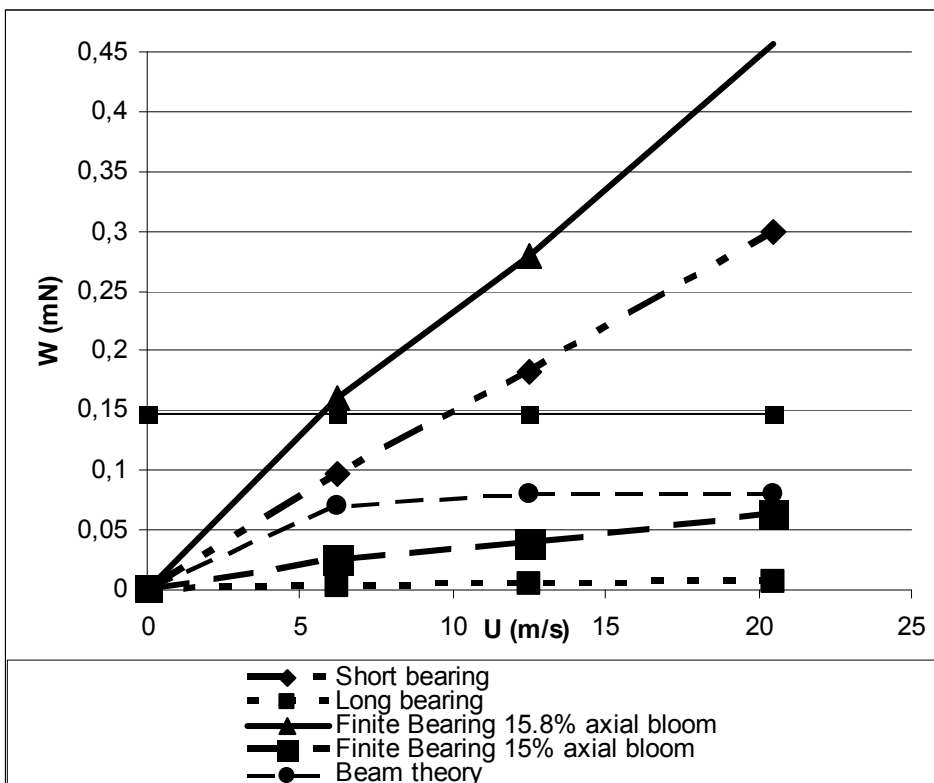

Figure 35: Forces on the bristle vs. speed for constant viscosity.

As illustrated in the figures, when the viscosity is constant, the hydrodynamic lift forces increase persistently as rotor surface speed increases. For ease of comparison, the results of only two axial bloom solutions by finite bearing method are plotted. When bristles are fully packed with no axial bloom, exposed bearing lengths at either side of the bristles are very limited, as staggered bristles in the adjacent rows block the penetration of oil pumped by the rotating shaft. As axial bloom increases bearing surface at each bristle tip increases. The pressure increases gradually at first. Then as further ends of the bristle gets exposed to lift pressure rapid increase takes place beyond 15 % axial bloom.

For a better comparison, Figure 35 presents calculated bristle reaction forces due to beam bending and blow down. Actual magnitude of the balancing forces is expected to be higher than the free beam bending, aided by the blow down forces. Actual blow down forces are expected to be lower than the calculated values due to restrictions by bristle mechanical interlocking and backing plate friction. Comparing with the magnitude of the bristle reaction forces, one can estimate the axial bloom for the case studied to be around 15.5%.

When the rotor surface speed increases, shear heating of the oil causes the oil viscosity to drop. In the absence of detailed thermal analysis, published temperature measurement data [40] in Figure 36 can be used for studying effect of increasing oil temperature with rotor speed.
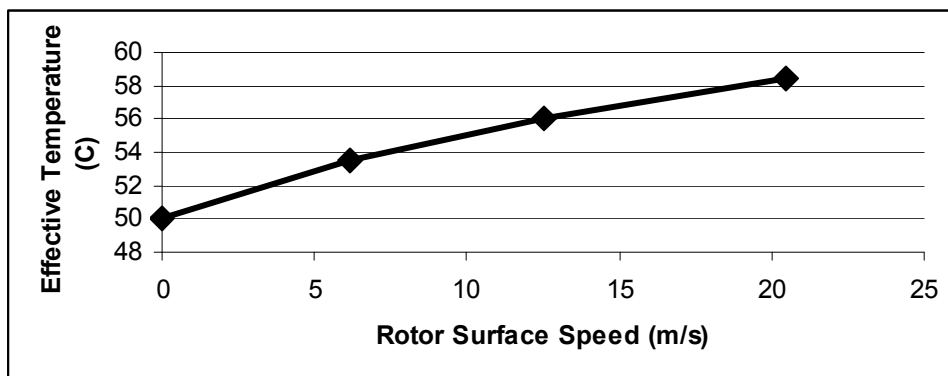
Figure 36: Effective temperature vs. rotor surface speed according to the measurement data.

As the speed and oil temperature increases, viscosity of the oil during the operation decreases. The change in viscosity with respect to the effective temperature for the test oil is given by [40]:

$$\mu = 0.028 e^{-0.0294(T-37.78)}$$

56

The structure of the formulae for the oil viscosity is generally the same, but the constants will change for different types of oil.

Normally, this graph is expected to decrease steeper with the speed increase as the temperature is exponentially related to viscosity. However, the temperature begins to stabilize after certain speed since the clearance also increases with speed. Therefore, above 12.5m/s surface speed, the graph settles down. Integrating the experimental oil temperatures, and including the shear heating of the oil analyses were repeated for each speed using the relevant oil temperatures from the available data. Figures 37, 38, 39 and 40 present analyses results using variable oil viscosity.

Figure 37: Hydrodynamic lift vs. speed for changing viscosity short bearing assumption.

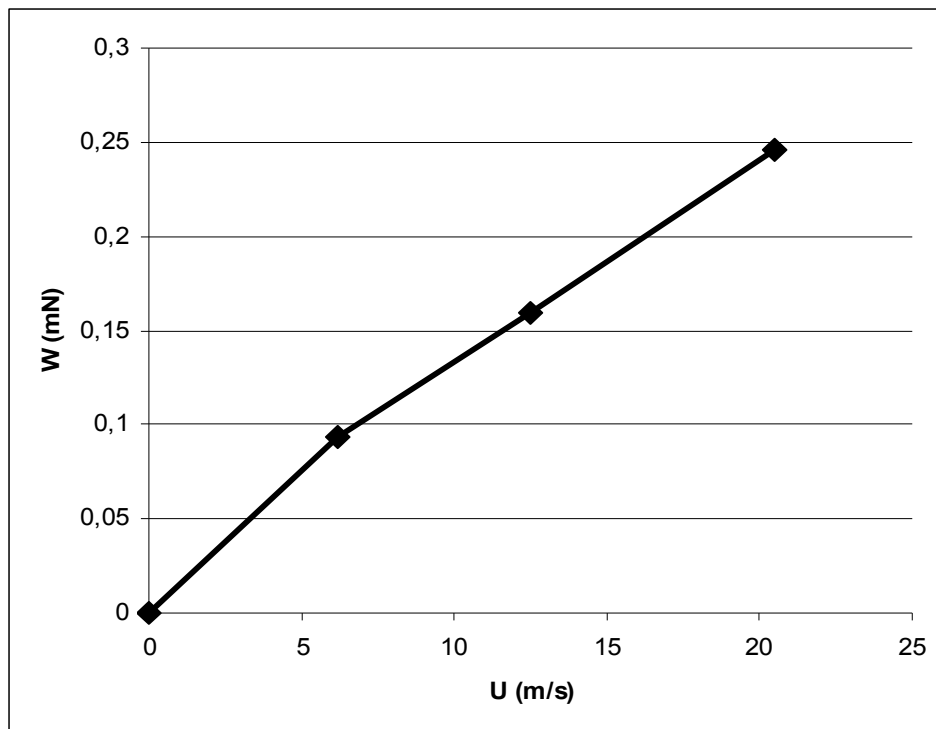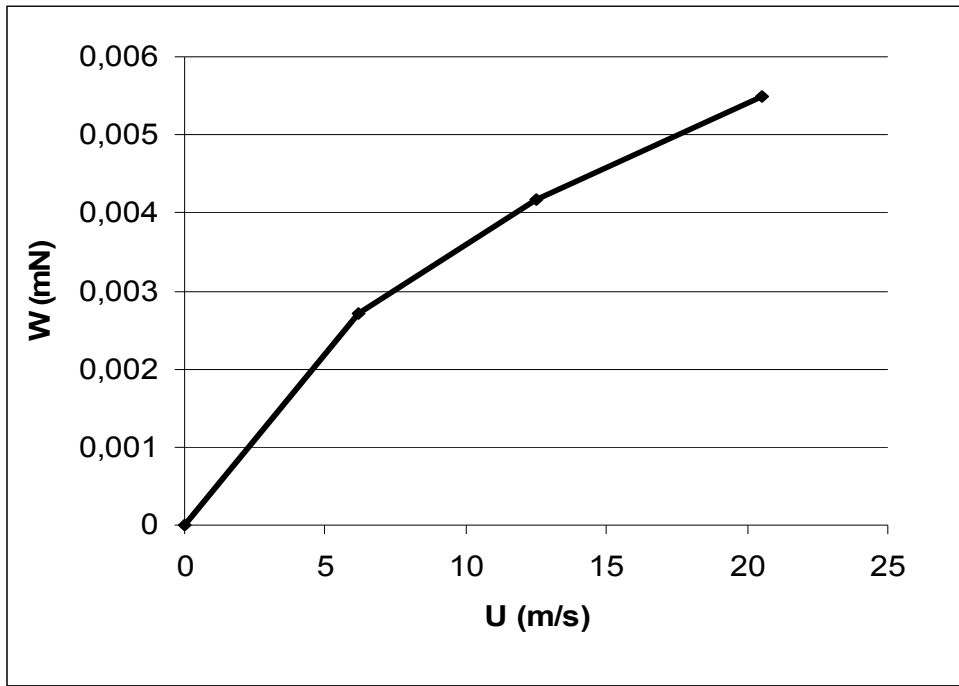Figure 38: Hydrodynamic lift vs. speed for changing viscosity long bearing assumption.
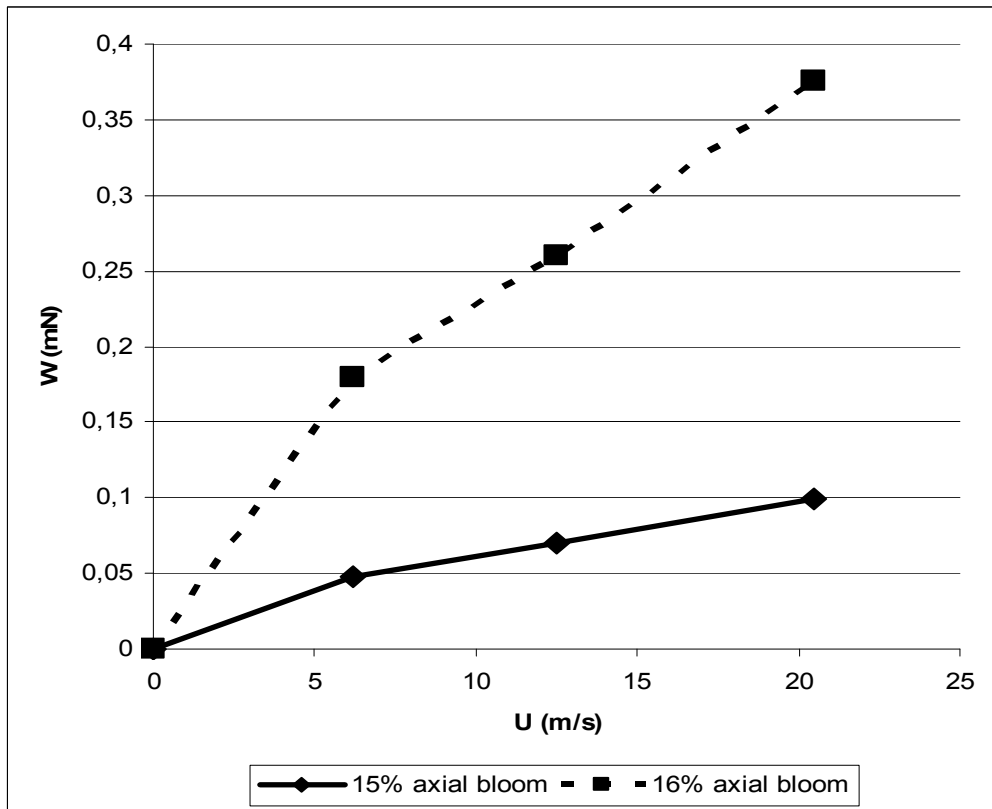

Figure 39: Hydrodynamic lift vs. speed for changing viscosity finite bearing assumption.
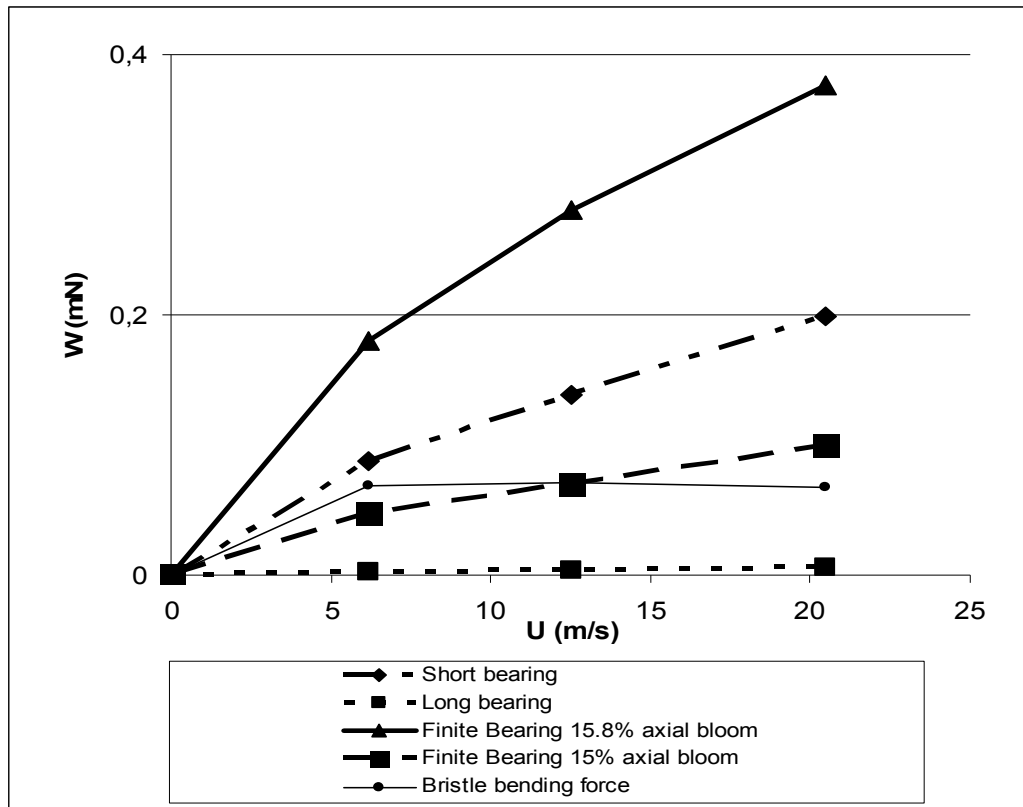
Figure 40: Forces on the bristle vs. speed for changing viscosity.

When results in Figure 40 are compared with Figure 35, it is observed that the lifting forces begin to stabilize as the rotor surface speed increases. As the speed increases, viscosity of the oil decreases due to the shear heating. Since the lift is a function of viscosity and speed, even though the speed increases, the lift force does not increase as much due to the decrease in the viscosity. The shear thinning effect stabilizes the amount of hydrodynamic lift clearance under bristle tips. This has a direct effect on the oil leakage flow. As a result, the oil leakage through the brush seal stabilizes after certain speed.

Overall, the long bearing approach underestimates the lift force with calculated force values below the simple beam bending solution. Since the space for the wedge action is very small and long bearing assumption does not allow the oil in the center sections to flow to the outer sections to contribute the generation of pressure like in finite bearing case, the hydrodynamic oil lift force cannot rise to an amount that would be sufficient to lift the bristle tips. It should also be noted that long bearing assumption loses its validity as moved away from the centerline.

Short bearing assumption is an idealized approach that is very useful as it provides a closed-form solution. It appears that the tendency of this analysis to

overestimate the lift force due to the full exposure of the analyzed bristle to hydrodynamic wedge action is somewhat nicely balanced with the tendency to underestimate peak pressure as neighboring bristles (upstream and downstream) are neglected, and oil is free to escape at either ends of the bristle. However, applicability of short bearing approach to various seal designs should be verified through comparison with further experimental data. Nevertheless, the short bearing analysis may be used for rule of thumb studies, since it has the ability to estimate the force with considerable closeness without the need for numerical computation.

Finite bearing assumption provides a more comprehensive solution keeping all the terms in the Reynolds equation. However, the effect of axial blooming in the staggered arrangement should be correctly modeled for an accurate result. The lift force difference between the solutions of the long bearing and finite bearing assumptions indicates that the oil flow in y direction has an important effect on the lift result of the finite bearing assumption. The effect of the axial bloom on the oil flow in y direction and its lifting effect should be investigated further and validated through experimental data.

6   CONCLUSION

The brush seal is a widely used and preferred sealing device in gas turbine engines. Its operation areas are expanding from air sealing to oil and oil mist sealing due to its effectiveness in controlling leakage flows between stationary parts and rotating shafts. When changing from air to oil sealing, nature of the problem changes from sealing of compressible, non-lubricating and low viscosity gas flows to incompressible, lubricating and high viscosity fluid flow. Due to the very small clearance, oil temperature rise and coking become main issues in addition to leakage performance. In oil sealing applications, high rotor surface speed and viscous sealing medium generate the hydrodynamic lift force which, in turn, creates a gap for oil leakage. This clearance is inversely correlated to oil temperature rise leading to the inverse correlation between the clearance and lifting force; therefore, it is a self-balancing process. Due to the difficulties in obtaining reliable measurements for the

bristle tip clearance around a rotating shaft, direct measurements and lift clearance data are not available. Instead, results of leakage measurements under certain rotor surface speed and pressure drop values for brush seals are used to estimate hydrodynamic lift clearance values.

In this work, lubrication and bearing theory have been applied to oil sealing applications of brush seals to study hydrodynamic lift clearance. Analytical solution approaches based on long bearing and finite bearing assumptions were formulized and short bearing solution approach was also illustrated. In the lack of any direct measurement and established procedure, some of the forces acting on the bristles were explained and calculated to facilitate comparison and validation of analytical results.

During analyses, constant oil viscosity conditions were used at first to demonstrate the behavior of the lifting force with respect to the rotor surface speed. Then, calculations were repeated for the variation of viscosity with rotor speed based on the published temperature measurements. All of the calculations were plotted to better illustrate behavior of each solution. Finally, results from various analytical approaches were compared; their performances in solving the bristle lift forces were discussed, and the needed further work was expressed. After detailed evaluation of brush seal oil lift behavior, following conclusions can be stated:

- Bristles in a typical brush seal are exposed to various load combinations under oil seal operation. To name a few axial sealing pressure, radial blow-down, mechanical interlocking and inclined-prop, inter-bristle and backing plate friction, hydrodynamic lift, beam deflection can be stated. The complicated nature of interacting multiple bristles under combined loading does not lend itself to an accurate analytical formulation. Therefore, it is necessary to use some simplifying approaches. In this sense, bearing theory can be exploited using the similarities based on plausible assumptions.

- The aim of this work is also to investigate possibility of obtaining a simplified closed form solution for oil lift. Any such solutions would be immensely helpful to engine designers who have to study what if scenarios and compare numerous seal designs.

- Hydrodynamic lift forces rapidly increase with rotor speed.

- The lift forces begin to stabilize as the rotor surface speed further increases due to the shear heating of oil. Since the lift is a function of viscosity and speed, even

61

though the speed increases, the lift does not increase indefinitely due to the decrease in the viscosity. Because the lift forces stabilize at higher speeds, the bristle tip clearance does not increase indefinitely either. This has a direct effect on the oil leakage flow.

- Depending on the axial bloom and penetration of oil pumped by the rotating shaft, short bearing or long bearing assumptions may be applicable to simplify the otherwise more complicated lubrication problem.

- The long bearing approach considers fully packed set of bristles, and assumes that only a very small tip portion of the bristles are exposed to the oil pumped by the shaft. Long bearing approach underestimates the lift forces. The calculated oil lift force does not exceed neither the beam bending force nor the blow-down force. Therefore, it can be concluded that the long bearing assumption may not be applicable to brush seal oil lift analyses.

- Short bearing approach considers only a single bristle. Since the bristle is assumed to be fully exposed to the lift pressure pumped by the rotating shaft, it is expected that the method will overestimate the lift force. On the other hand, because the neighboring bristles are ignored, oil squeezed by the rotor under the bristle freely escapes to either side implying lower than actual lift pressures. The results indicate that the two contradicting effects nicely balance each other to yield a reasonable lift force estimate as compared to the more detailed finite bearing approach.

- Finite bearing approach is more comprehensive including all the terms in Reynolds Equation. However, only a numerical solution can be obtained. Because of the fact that position of the bristles in the adjacent rows determine the integration limits, solution depends on the axial bloom (or degree of oil penetration) present. Therefore, solutions for various axial bloom levels have been calculated and presented. As expected, lift force estimates vary from below long bearing results to over short bearing calculations depending on the oil penetration.

Overall, finite bearing approach is more realistic attempt to solve for full Reynolds Equation. However, only a numerical solution is available. The actual magnitude of the hydrodynamic lift clearance cannot be determined until the bristle tip reaction forces are known. Calculation of bristle tip reaction forces requires very detailed further analyses which are beyond the scope of this study. However, bulk

comparisons with known beam forces indicate that the solution obtained by short bearing assumption is a good compromise. The fact that short bearing analysis allows a closed form solution will prove very useful to sealing community. This will allow analysis of what if scenarios before going through the expensive process of fabricating and testing of a final seal design. However, wider applicability of short bearing formulation should be further evaluated through more testing and comparison of other seal designs.

7   REFERENCES

[1]   Steinetz, B. M. and Hendricks, R. C., "Engine Seal Technology Requirements to Meet NASA's Advanced Subsonic Technology Program Goals," **NASA/TM-1994-106582**, **AIAA–94–2698**, (1994).

[2]   Dinc, S., Demiroglu, M., Turnquist, N., Mortzheim, J., Goetze, G., Maupin, J., Hopkins, J., Wolfe, C. and Florin, M., "Fundamental Design Issues of Brush Seals for Industrial Applications," *ASME Trans. J. Turbomachinery*, **124**, pp. 293-300, (2004).

[3]   Bhate, N., Thermos, A. C., Aksit, M. F., Demiroglu, M. and Kizil, H., "Non-Metallic Brush Seals For Gas Turbine Bearings," ASME Turbo Expo Conference Paper **ASME GT2004-54296**, (2004).

[4]   Aksit, M. F., Bhate, N., Bouchard, C., Demiroglu, M. and Dogu, Y., "Evaluation of Brush Seal Performance for Oil Sealing Applications," AIAA/ASME/SAE/ASEE 39th Joint Propulsion Conference Paper **AIAA-2003-4695**, (2003).

[5]   Shapiro, W., "Film Riding Brush Seal Preliminary Studies," NASA Seal Workshop 2002.

[6]   Chupp, R. E. and Loewenthal, R. G., "Brush Seals Can Improve Power Plant Efficiency By One-fourth Of A Percentage," *Tribology & Lubrication Technology*; Jun 1997; 53, 6; ProQuest Science Journals pp. 10-14, (1997).

[7]   Aksit, M. F., "A Computational Study of Brush Seal Contact Loads with Friction," Ph.D. Thesis, Rensselaer Polytechnic Institute, Troy, NY, USA, (1998).

[8]   Gorelev, G. M., Reznik, V. E. and Tsibizov, V. I., "Experimental Study Of Brush Seal Flow Characteristics And Comparison With A Labyrinth Seal," *Izvestiya VUZ. Aviatsionnaya Tekhnika*, **31**, pp. 43-46, (1988).

[9]   Chen, L. H., Wood, P. E., Jones, T. V. and Chew, J. W., "Detailed Experimental Studies of Flow in Large Scale Brush Seal Model and a Comparison With CFD Predictions," *ASME Trans. J. Eng. for Gas Turbines and Power*, **122**, pp. 672-679, (2000).

[10] Crudgington, P. F., and Bowsher, A., "Brush Seal Pack Hysteresis," AIAA/ASME/SAE/ASEE 38th Joint Propulsion Conference Paper **AIAA-2002-3794**, (2002).

[11] Duran, E. T., Aksit, M. F. and Dogu, Y., "Effect Of Shear Heat On Hydrodynamic Lift Of Brush Seals In Oil Sealing,", AIAA/ASME/SAE/ASEE 42nd Joint Propulsion Conference Paper, **AIAA-2006-4755**, (2006)

[12] Owen, A. K., Jones, T. V., Guo, S. M., and Hogg, S., "An Experimental and Theoretical Study of Brush Seal and Shaft Thermal Interaction," ASME Paper No. **GT-2003-38276**, (2003).

[13] Chew, J. W., and Guardino, C., "Simulation of Flow and Heat Transfer in the Tip Region of a Brush Seal," *Int. J. Heat Fluid Flow*, **25(4)**, pp. 649–658, (2004).

[14] Dogu, Y. and Aksit, M. F., "Brush Seal Temperature Distribution Analysis," *Proc. ASME Turbo Expo 2005 Technical Congress*, **ASME GT2005-69120**, (2005).

[15] Zhao, H. and Stango, R. J., "Effect of Flow-Induced Radial Load on Brush Seal/Rotor Contact Mechanics," ASME Trans. J. Trib., **126**, pp. 208-215, (2004).

[16] Dogu, Y., "Investigation Of Brush Seal Flow Characteristics Using Bulk Porous Medium Approach," *Proc. ASME Turbo Expo 2003 Technical Congress*, **ASME GT2003_38970**, (2003).

[17] Foley, M. E., "Retractable Brush Seals Allow Sweeping Improvements In Steam Turbine Efficiency," *Modern Power Systems*, Jul 2000; 20, 7; Career and Technical Education pp. 37-39, (2000).

[18] Chupp, R. E., Aksit, M. F., Ghasripoor, F. and Turnquist, N. A., "Advanced Seals For Industrial Turbine Applications," AIAA/ASME/SAE/ASEE Joint Propulsion Conference Paper **AIAA-2001-3626**, (2001).

[19] Mayer, R. R., Aksit, M. F., and Bagepalli, B. S., "Brush Seal for a Bearing Cavity," US Patent No. US6502824B2, (2003).

[20] Aksit, M. F., Dinc, O. S., and Mayer, R. R., "Brush Seal and Machine Having a Brush Seal," US Patent No. US6406027B1, (2002).

[21] Mayer, R. R., Bagepalli, B. S., and Aksit, M. F., "Low Flow Fluid Film Seal for Hydrogen Cooled Generators," US Patent No. US6378873B1, (2002).

[22] Bagepalli, B. S., Aksit M. F., and Mayer, R. R., "Brush Seal and Rotary Machine Including Such Brush Seal," US Patent No. US6257588B1, (2001).

[23]   Fellenstein, J. A., DellaCorte, C., Moore, K. D. and Boyes, E., "High Temperature Brush Seal Tuft Testing Of Selected Nickel-Chrome And Cobalt-Chrome Superalloys," **NASA/-TM-10497**, AIAA/SAE/ASME/ASEE 33rd Joint Propulsion Conference Paper **AIAA-97-2634**, (1997).

[24]   Ferguson, J.G., "Brushes as High Performance Gas Turbine Seals," ASME Gas Turbine and Aeroengine Congress Paper **ASME 88-GT-182**, (1988).

[25]   Steinetz, B. M., Hendricks, R. C., and Munson, J., ''Advanced Seal Technology Role in Meeting Next Generation Turbine Engine Goals,'' **NASA/ TM-1998-206961**, AVT-PPS Paper No. 11, (1998).

[26]   Ingistov, S., "Compressor Discharge Brush Seal for Gas Turbine Model 7EA," *ASME Trans. J. Turbomachinery*, **124**, pp. 301-305, (2002).

[27]   Ingistov, S., "Power Augmentation and Retrofits of Heavy Duty Industrial Turbines model 7EA," bp/Watson Cogeneration Co. , Carson California, (2002).

[28]   Braun, M., and Canacci, V. A., "Flow Visualization and Motion Analysis for a Series of Four Sequential Brush Seals," AIAA/SAE/ASME/ASEE 26th Joint Propulsion Conference Paper **AIAA 90-2482**, (1990).

[29]   Braun, M. J., Canacci, V. A., and Hendricks, R. C., "Flow Visualization and Quantitative Velocity and Pressure Measurements in Simulated Single and Double Brush Seals," *Tribol. Trans.*, **34**, pp. 70–80, (1991).

[30]   Carlile, J.A., Hendricks, R.C. and Yoder, D.A., "Brush Seal Leakage Performance with Gaseous Working Fluids at Static and Low Rotor Speed Conditions," *ASME Trans. J. Eng. for Gas Turbines and Power*, 115, pp 397-403, (1993).

[31]   Hendricks, R.C., Carlile, J.A., and Liang, D.A., "Some sealing concepts - a review, part b: brush seal systems*," Proc. of the 4th Int. Symp. on Transport Phenomena and Dynamics of Rotating Machinery (ISROMAC-4)*, Honolulu, HI, pp 222-227, (1992).

[32]   Ingistov, S., "Power Augmentation and Retrofits of Heavy Duty Industrial Turbines model 7EA," Proc. Of Power-Gen International Conference, Las Vegas, NV, (2001).

[33]   Wood, P. E., and Jones, T. V., "A Test Facility for the Measurement of Torques at the Shaft to Seal Interface in Brush Seals," ASME Paper No. 97-GT-184, (1997).

[34]   Hendricks, R. C., Schlumberger, S., Braun, M. J., Choy, F., and Mullen, R. L., "A Bulk Flow Model of a Brush Seal System," ASME Gas Turbine and Aeroengine Congress Paper ASME 91-GT-325, (1991).
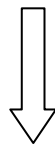
[35]   Bayley, F. J., and Long, C. A., ''A Combined Experimental and Theoretical Study of Flow and Pressure Distributions in a Brush Seal,'' *ASME J. Eng. for Gas Turbines and Power*, **115**, pp. 404–410, (1993).

[36]   Chew, J. W., Lapworth, B. L. and Millener, P. J., "Mathematical Modeling of Brush Seals," Int. J. Heat and Fluid Flow, 16, pp 493-500, (1995).

[37]   Chen, L. H., Wood, P. E., Jones, T. V., and Chew, J. W., ''An Iterative CFD and Mechanical Brush Seal Model and Comparison With Experimental Results," *ASME J. Eng. for Gas Turbines and Power*, **121**, pp. 656–662, (1999).

[38]   Modi, V., "Modeling Bristle Lift-Off in Idealized Brush Seal Configurations," Proc. Of the 4th Int. Symp. On Transport Phenomena and Dynamics of Rotating Machinery (ISROMAC-4), Honolulu, HI, (1992).

[39]   Sharatchandra, M. C., and Rhode, D. L., "Computed Effects of Rotor-Induced Swirl on Brush Seal Performance – Part 2: Bristle Force Analysis," ASME Trans. J. Trib., **118**, pp 920-926, (1996).

[40]   Aksit, M.F., Dogu, Y., Tichy, J. A. and Gursoy M., "Hydrodynamic Lift of Brush Seals In Oil Sealing Applications," Proc. 40th AIAA/ASME/SAE/ASEE Joint Propulsion Conference & Exhibit, Fort Lauderdale, Florida, AIAA-2004-3721, (2004).

[41]   Young, W. C., "Roark's Formulas for Stress and Strain," 6th ed., McGraw-Hill, Inc., New York, (1989).

[42]   Wood, P. E., ''Investigation of Contact Forces, Flow, Pressure, Hysteresis and Frictional Effects in Brush Seals,'' dissertation, University of Oxford, UK, (1998).

[43]   Turner, M. T., Chew, J. W., and Long, C. A., ''Experimental Investigation and Mathematical Modeling of Clearance Brush Seals,'' ASME J. Eng. for Gas Turbines and Power, **120**, pp. 573-579, (1998).

[44]   Braun, M.J., Hendricks, R.C. and Canacci, V., "Flow Visualization in a Simulated Brush Seal," ASME Gas Turbine and Aeroengine Congress Paper **ASME 90-GT-217**, (1990).

[45]   Braun, M.J., Canacci, V.A., and Hendricks, R.C., "Flow Visualization and Quantitative Velocity and Pressure Measurements in Simulated Single and Double Brush Seals," *Trib. Trans.*, **34**, pp 70-80, (1991).

[46]   Turner, M.T., Chew, J.W. and Long, C.A., "Experimental Investigation and Mathematical Modeling of Clearance Brush Seals," ASME Gas Turbine and Aeroengine Congress Paper **ASME 97-GT-282**, (1997).

[47]   http://www.mobil.com/USA-English/Lubes/PDS/GLXXENINDMOMobil_DTE_20.asp#TypicalPropertyTitle

[48]   Bhushan, B., "Modern Tribology Handbook," 29th ed., CRC Press, New York, 2001.

8   APPENDICES

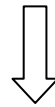## 8.1   Step-by-step Calculations for Long-Bearing Solution

$$\frac{\partial}{\partial x}\left(\frac{\rho h^3}{\mu}\frac{\partial P}{\partial x}\right) = 6\,U\frac{\partial(\rho h)}{\partial x}$$

Since this paper does not deal with shear heating in the bristle pack, a constant effective temperature is considered. Therefore, ρ (viscosity) is constant.

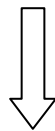$$\frac{\partial}{\partial x}\left(h^3\frac{\partial P}{\partial x}\right) = 6\mu\,U\frac{\partial h}{\partial x}$$

Integrate once to get

$$h^3\frac{\partial P}{\partial x} = 6\mu\,U\,h + C_1$$

$$C_1 = -h_m\,6\mu\,U \qquad \text{(where } h_m \text{ is the h value at } \partial P/\partial x = 0)$$

$$\frac{\partial P}{\partial x} = 6\mu\,U\left(\frac{h-h_m}{h^3}\right)$$

Integrating again with respect to x

$$P = 6\mu U \int_{LimitLow}^{x}\frac{h(x)-h_m}{h^3(x)}dx + C_2$$

We need to find h_m and c_2:

$P = P_a$ @ x = LimitHigh, and x = LimitLow

$$P\Big|_{LimitHigh} - P\Big|_{LimitLow} = 0 = 6\mu\,\mathrm{U}\left(\int_{LimitLow}^{LimitHigh}\frac{dx}{h^2(x)} - h_m\int_{LimitLow}^{LimitHigh}\frac{dx}{h^3(x)}\right)$$

$$h_m = \frac{\displaystyle\int_{LimitLow}^{LimitHigh}\frac{dx}{h^2(x)}}{\displaystyle\int_{LimitLow}^{LimitHigh}\frac{dx}{h^3(x)}}$$

Now plug in the h function defined before

$$h = H - \frac{\sqrt{R_b^2 - y^2}}{\sin\theta} - \frac{1}{\tan\theta}x$$

|-----------a------------|-----b-----|

$$a = H - \frac{\sqrt{R_b^2 - y^2}}{\sin\theta}$$

$$b = -\frac{1}{\tan\theta}$$

$$\int\frac{dx}{(a+bx)^2} = -\frac{1}{-\dfrac{1}{\tan\theta}(a+bx)} = \frac{\tan\theta}{a+bx}$$

$$\int\frac{dx}{(a+bx)^3} = -\frac{1}{2\dfrac{-1}{\tan\theta}(a+bx)^2} = \frac{\tan\theta}{2(a+bx)^2}$$

$$h_m = \frac{\tan\theta\left(\dfrac{1}{a+bLimitHigh} - \dfrac{1}{a+bLimitLow}\right)}{\dfrac{\tan\theta}{2}\left(\dfrac{1}{(a+bLimitHigh)^2} - \dfrac{1}{(a+bLimitLow)^2}\right)}$$

$$h_m = \frac{2}{\left[\dfrac{1}{a + bLimitHigh} + \dfrac{1}{a + bLimitLow}\right]}$$

$$h_m = \frac{2(a + bLimitHigh)(a + bLimitLow)}{2a + b(LimitHigh + LimitLow)}$$

Where

$$LimitLow = \frac{-2R_b + \sqrt{R_b^2 - y^2}}{\cos\theta} - 0.05\frac{2R_b}{\cos\theta}$$

$$LimitHigh = \frac{-\sqrt{R_b^2 - y^2}}{\cos\theta}$$

$$h = H - \frac{\sqrt{R_b^2 - y^2}}{\sin\theta} - \frac{1}{\tan\theta}x$$

$$P\Big|_{LimitLow} = P\Big|_{LimitHigh} = P_a = C_2$$

$$P - P_a = 6\mu\, U\left(\int_{LimitLow}^{x} \frac{dx}{h^2(x)} - h_m \int_{LimitLow}^{x} \frac{dx}{h^3(x)}\right)$$

$$P - P_a = 6\mu\, U\left|\begin{array}{l} \dfrac{\tan\theta}{a + bx} - \dfrac{\tan\theta}{a + bLimitLow} - h_m\dfrac{\tan\theta}{2(a + bx)^2} \\[2ex] + h_m\dfrac{\tan\theta}{2(a + bLimitLow)^2} \end{array}\right|$$

$$P - P_a = 6\mu\, U\tan\theta\left(\begin{array}{l} \dfrac{1}{a + bx} - \dfrac{1}{a + bLimitLow} \\[2ex] -\dfrac{h_m}{2(a + bx)^2} + \dfrac{h_m}{2(a + bLimitLow)^2} \end{array}\right)$$

$$P - P_a = 6\mu\,U\tan\theta\left|\frac{\dfrac{1}{a+bx}-\dfrac{1}{a+bLimitLow}-\dfrac{(a+bLimitHigh)(a+bLimitLow)}{2a+b\big(LimitHigh+LimitLow\big)}}{\left(\dfrac{1}{(a+bx)^2}-\dfrac{1}{(a+bLimitLow)^2}\right)}\right|$$

Where, P_a is the ambient pressure.

$$a = H - \frac{\sqrt{R_b{}^2 - y^2}}{\sin\theta}$$

$$b = -\frac{1}{\tan\theta}$$

$$LimitLow = \frac{-2R_b + \sqrt{R_b{}^2 - y^2}}{\cos\theta} - 0.05\frac{2R_b}{\cos\theta}$$

$$LimitHigh = \frac{-\sqrt{R_b{}^2 - y^2}}{\cos\theta}$$

$$W = 2\int_{y=0}^{R_b}\int_{x=LimitLow}^{LimitHigh}\big(P - P_a\big)dxdy$$

$$W = 12\mu\,U\tan\theta\int_{y=0}^{R_b}\int_{x=LimitLow}^{LimitHigh}\left|\frac{\dfrac{1}{a+bx}-\dfrac{1}{a+bLimitLow}-\dfrac{(a+bLimitHigh\,)(a+bLimitLow\,)}{2a+b\big(LimitLow+LimitHigh\big)}}{\left(\dfrac{1}{(a+bx)^2}-\dfrac{1}{(a+bLimitLow\,)^2}\right)}\right|dxdy$$

$$W = 12\mu\,\mathrm{U}\tan\theta \int\limits_{y=0}^{R_b} \left(\int\limits_{x=LimitLow}^{LimitHigh} \left| \frac{\dfrac{1}{a+bx} - \dfrac{1}{a+bLimitLow}}{-\dfrac{(a+bLimitHigh)(a+bLimitLow)}{2a+b(LimitLow+LimitHigh)}} \left(\frac{1}{(a+bx)^2} - \frac{1}{(a+bLimitLow)^2} \right) \right| dx \right) dy$$

$$W = 12\mu\,\mathrm{U}\tan\theta \int\limits_{y=0}^{R_b} \left| \frac{\dfrac{\log\left(\dfrac{a+bLimitHigh}{a+bLimitLow}\right)}{b} - \dfrac{LimitHigh-LimitLow}{a+bLimitLow}}{-\dfrac{(a+bLimitHigh)(a+bLimitLow)}{2a+b(LimitLow+LimitHigh)}} \left(\frac{-(a+bLimitLow)+(a+bLimitHigh)}{b(a+bLimitHigh)(a+bLimitLow)} - \frac{LimitHigh-LimitLow}{(a+bLimitLow)^2} \right) \right| d.$$

$$W = 12\mu\,\mathrm{U}\tan\theta \int\limits_{y=0}^{R_b} \left| \frac{\dfrac{\log\left(\dfrac{a+bLimitHigh}{a+bLimitLow}\right)}{b} - \dfrac{LimitHigh-LimitLow}{a+bLimitLow}}{-\dfrac{(a+bLimitHigh)(a+bLimitLow)}{2a+b(LimitLow+LimitHigh)}} \left(\frac{LimitHigh-LimitLow}{(a+bLimitHigh)(a+bLimitLow)} - \frac{LimitHigh-LimitLow}{(a+bLimitLow)^2} \right) \right| dy$$

$$W = 12\mu\,\mathrm{U}\tan\theta \int\limits_{y=0}^{R_b} \left| \frac{\dfrac{\log\left(\dfrac{a+bLimitHigh}{a+bLimitLow}\right)}{b} - \dfrac{LimitHigh-LimitLow}{a+bLimitLow}}{-\dfrac{(a+bLimitHigh)(a+bLimitLow)}{2a+b(LimitLow+LimitHigh)} \dfrac{LimitHigh-LimitLow}{(a+bLimitLow)}} \left(\frac{1}{a+bLimitHigh} - \frac{1}{a+bLimitLow} \right) \right| dy$$

$$W = 12\mu\,\mathrm{U}\tan\theta \int\limits_{y=0}^{R_b} \left\{ \frac{\log\left(\frac{a+bLimitHigh}{a+bLimitLow}\right)}{b} - \frac{LimitHigh - LimitLow}{a+bLimitLow} + \frac{(a+bLimitHigh)(LimitHigh - LimitLow)}{2a+b(LimitLow + LimitHigh)}\left(\frac{b(LimitHigh - LimitLow)}{(a+bLimitHigh)(a+bLimitLow)}\right) \right\} dy$$

$$W = 12\mu\,\mathrm{U}\tan\theta \int\limits_{y=0}^{R_b} \left\{ \frac{\log\left(\frac{a+bLimitHigh}{a+bLimitLow}\right)}{b} - \frac{LimitHigh - LimitLow}{a+bLimitLow} + \frac{b(LimitHigh - LimitLow)^2}{(2a+b(LimitLow + LimitHigh))(a+bLimitLow)} \right\} dy$$

$$W = 12\mu\,\mathrm{U}\tan\theta \int\limits_{y=0}^{R_b} \left\{ \frac{\log\left(\frac{a+bLimitHigh}{a+bLimitLow}\right)}{b} - \frac{LimitHigh - LimitLow}{a+bLimitLow}\left(1 - \frac{b(LimitHigh - LimitLow)}{2a+b(LimitLow + LimitHigh)}\right) \right\} dy$$

$$W = 12\mu\,\mathrm{U}\tan\theta \int\limits_{y=0}^{R_b} \left\{ \frac{\log\left(\frac{a+bLimitHigh}{a+bLimitLow}\right)}{b} - \frac{LimitHigh - LimitLow}{a+bLimitLow}\left(\frac{2a+bLimitLow+bLimitHigh-bLimitHigh+bLimitLow}{2a+b(LimitLow + LimitHigh)}\right) \right\} dy$$

$$W = 12\mu\,\mathrm{U}\tan\theta \int\limits_{y=0}^{R_b} \left\{ \frac{\log\left(\frac{a+bLimitHigh}{a+bLimitLow}\right)}{b} - \frac{LimitHigh - LimitLow}{a+bLimitLow}\left(\frac{2a+2bLimitLow}{2a+b(LimitLow + LimitHigh)}\right) \right\} dy$$

$$W = 12\mu\,\mathrm{U}\tan\theta \int\limits_{y=0}^{R_b} \left(\frac{\log\left(\dfrac{a+bLimitHigh}{a+bLimitLow}\right)}{b} - 2\frac{LimitHigh - LimitLow}{2a + b(LimitLow + LimitHigh)} \right) dy$$

$$a = H - \frac{\sqrt{R_b^2 - y^2}}{\sin\theta}$$

$$b = \frac{-1}{\tan\theta}$$

$$LimitLow = \frac{-2R_b + \sqrt{R_b^2 - y^2}}{\cos\theta} - 0.05\frac{2R_b}{\cos\theta} = \frac{-2R_b + \sqrt{R_b^2 - y^2} - 0.1R_b}{\cos\theta}$$

$$LimitHigh = \frac{-\sqrt{R_b^2 - y^2}}{\cos\theta}$$

$$W = 12\mu\,\mathrm{U}\tan\theta \int\limits_{y=0}^{R_b} \left(\frac{\log\left(\dfrac{H - \dfrac{\sqrt{R_b^2 - y^2}}{\sin\theta} + \dfrac{-1}{\tan\theta}\dfrac{-\sqrt{R_b^2 - y^2}}{\cos\theta}}{H - \dfrac{\sqrt{R_b^2 - y^2}}{\sin\theta} + \dfrac{-1}{\tan\theta}\dfrac{-2R_b + \sqrt{R_b^2 - y^2} - 0.1R_b}{\cos\theta}}\right)}{\dfrac{-1}{\tan\theta}} - 2\frac{\dfrac{-\sqrt{R_b^2 - y^2}}{\cos\theta} - \dfrac{-2R_b + \sqrt{R_b^2 - y^2} - 0.1R_b}{\cos\theta}}{2H - \dfrac{2\sqrt{R_b^2 - y^2}}{\sin\theta} + \dfrac{-1}{\tan\theta}\left(\dfrac{-2R_b + \sqrt{R_b^2 - y^2} - 0.1R_b}{\cos\theta} + \dfrac{-\sqrt{R_b^2 - y^2}}{\cos\theta}\right)} \right) dy$$

$$W = 12\mu\,\mathrm{U}\tan\theta \int\limits_{y=0}^{R_b} \left(-\tan\theta\log\left(\frac{H - \dfrac{\sqrt{R_b^2 - y^2}}{\sin\theta} + \dfrac{\sqrt{R_b^2 - y^2}}{\sin\theta}}{H - \dfrac{-2R_b + 2\sqrt{R_b^2 - y^2} - 0.1R_b}{\sin\theta}}\right) - 2\frac{-\dfrac{-2R_b + 2\sqrt{R_b^2 - y^2} - 0.1R_b}{\cos\theta}}{2H - \dfrac{2\sqrt{R_b^2 - y^2}}{\sin\theta} - \dfrac{-2R_b - 0.1R_b}{\sin\theta}} \right) dy$$

$$W = 12\mu\,\mathrm{U}\tan\theta \int_{y=0}^{R_b} \left(-\tan\theta \log\left(\frac{H\sin\theta}{H\sin\theta + 2R_b - 2\sqrt{R_b^2 - y^2} + 0.1R_b}\right) + 2\tan\theta\,\frac{-2R_b + 2\sqrt{R_b^2 - y^2} - 0.1R_b}{2H\sin\theta - 2\sqrt{R_b^2 - y^2} + 2R_b + 0.1R_b} \right) dy$$

$$W = 12\mu\,\mathrm{U}\tan^2\theta \int_{y=0}^{R_b} \left(-\log\left(\frac{H\sin\theta}{H\sin\theta + 2R_b - 2\sqrt{R_b^2 - y^2} + 0.1R_b}\right) + 2\,\frac{-2R_b + 2\sqrt{R_b^2 - y^2} - 0.1R_b}{2H\sin\theta - 2\sqrt{R_b^2 - y^2} + 2R_b + 0.1R_b} \right) dy$$

$$W = 12\mu\,\mathrm{U}\tan^2\theta \int_{y=0}^{R_b} \left(-\log\left(\frac{H\sin\theta}{H\sin\theta + 2.1R_b - 2\sqrt{R_b^2 - y^2}}\right) - 2 + \frac{4H\sin\theta}{2H\sin\theta - 2\sqrt{R_b^2 - y^2} + 2.1R_b} \right) dy$$